A

Thesis

On

HYDRODYNAMIC STUDY OF INVERSE FLUIDIZATION: CFD ANALYSIS

Submitted By

N. Shailaja

(211CH1039)

Under the Supervision of

Dr. Abanti Sahoo

In partial fulfilment for the award of the Degree of

Master of Technology

In

Chemical Engineering

Department Of Chemical Engineering

National Institute Of Technology

Rourkela, Odisha, India

May 2013

CERTIFICATE

Certified that this Project thesis entitled "***Hydrodynamic Studies of Inverse Fluidized Bed: CFD Analysis"*** by **N. Shailaja (211CH1039)** during the year 2012- 2013 in partial fulfillment of the requirements for the award of the Degree of Master of Technology in Chemical Engineering at National Institute of Technology, Rourkela has been carried out under my supervision. To the best of my knowledge, the matter embodied in the report has not been submitted to any other University/Institute for the award of any Degree.

Date: **Supervisor:**

Dr. Abanti Sahoo
Associate Professor
Department of Chemical Engineering
National Institute of Technology
Rourkela.

ACKNOWLEDGEMENT

I feel immense pleasure and privilege to express my deep sense of gratitude and feel indebted towards all those people who have helped, inspired and encouraged me during the preparation of this report.

I am grateful to my supervisor, Prof. Abanti Sahoo, for her kind support, guidance and encouragement throughout the project work, also for introducing to this topic. I would also like to thank HOD, Prof. R. K. Singh for his kind help to make this report complete. I am also thankful to all the staff and faculty members of Chemical Engineering Department, National Institute of Technology, Rourkela for their consistent encouragement. Last but not the least, I would like to thank whole heartedly my parents and family members whose love and unconditional support, both on academic and personal front, enabled me to see the light of this day.

N. Shailaja

211CH1039

Table of Contents

Title……... i

Certificate…….. ii

Acknowledgement…… iii

Contents…… iv

List of Tables…… v

List of figures…… vii

Nomenclature…… viii

Abstract…… ix

1. Introduction……..... 1

1.1. Advantages of inverse fluidization……..... 1

1.2. Application of inverse fluidization……..... 2

1.3. Importance of CFD for inverse fluidization……..... 3

1.4. Objective of the present work……..... 4

1.5. Outline of the report..... 4

2. Literature Survey……..... 7

2.1. Hydrodynamic study of inverse fluidized bed……..... 8

2.2. CFD modeling done on conventional three phase fluidized beds……..... 13

3. Experimental Set-up……..... 16

3.1. Experimental set-up……..... 16

3.2. Parts of set-up……..... 17

3.3. Experimental procedure……..... 18

4. Computational Fluid Dynamics……..... 20

4.1. Computational Fluid Dynamic Codes…….. 21

4.2. Limitations of CFD……..... 21

4.3. CFD approaches in multiphase flow……..... 22

4.4. Conservation equations……..... 23

4.5. Choosing a multiphase model……..... 27

4.6. Geometry and meshing……... 27

4.7. Boundary and initial conditions…….. 29

4.8. Solution methods……..... 30

5. Results……..... 32

5.1. Contours of volume fraction of solids……..... 32
5.2. Phase dynamics……..... 33
5.3. Velocity vector of solid and fluid phases……..... 34
5.4. Bed expansion……..... 37
5.5. Pressure drop……..... 38
6. Conclusion……..... 42
References…… 45

List of Tables

Table No.	Topic	Page No.
Table 2.1.	Hydrodynamic study on inverse fluidized bed …….....	8
Table 4.1.	Mesh parameters ……....	29
Table 4.2.	Phase parameters…….	29
Table 4.3.	Solution methods …….....	30

List of Figures

Figure No.	Caption	Page No.
Figure 2.1.	Flow regime diagram for inverse gas-liquid-solid fluidized bed……	9
Figure 2.2.	Determination of minimum fluidization velocity …….....	10
Figure 2.3.	Variation of bed height with superficial gas velocity.....	11
Figure 2.3.	Variation of gas volume fraction with superficial gas velocity.....	12
Figure 3.1.	Schematic diagram of the experimental set-up.....	16
Figure 4.1.	Geometry.....	28
Figure 4.2.	Meshing at the split zone area.....	28
Figure 5.1.	Contours of volume fraction at varying intervals.....	33
Figure 5.2.	Contours of volume fraction of solid, liquid and air.....	34
Figure 5.3.	Velocity vector of liquid phase.....	35
Figure 5.4.	Velocity vector of liquid phase at different sections.....	35
Figure 5.5	Velocity vector of air at the middle, top and bottom sections.....	36
Figure 5.6.	Variation of solid volume fraction along bed in axial direction.....	37
Figure 5.7.	Variation of gas hold-up with radial direction at different bed heights..	38
Figure 5.8.	Variation of gas hold-up with increasing liquid velocity along axial direction……....	38
Figure 5.9.	Variation of gas volume fraction with variation in gas velocity…….	39
Figure 5.10.	Pressure variation with liquid velocity at varying gas velocities…...…	39

Nomenclature

U_{mf}:	Minimum fluidization velocity
ε_g:	Gas hold-up
U:	Superficial gas velocity
V_q:	Volume of phase q
α_q:	Volume fraction of phase q
$\vec{\rho}_q$:	Effective density of phase q, Kg m^{-3}
ρ_q:	Physical density of the phaseq, Kg m^{-3}
$\vec{v}_q$:	Velocity of phase *q*, m s^{-1}
$\dot{m}_{pq}$:	Mass transfer from phase *q* to phase *p*
$\dot{m}_{qp}$:	Mass transfer from phase *p* to phase *q*
S_q:	Source term
$\bar{\bar{\tau}}_q$:	q^{th} phase stress-strain tensor, Pa
μ_q:	Shear viscosity of the phase *q*, m s^{-1}
λ_q:	Bulk viscosity of phase *q*, m s^{-1}
$\vec{F}_q$:	External body force, N
$\vec{F}_{lift,q}$:	Lift force, N
$\vec{F}_{vm,q}$:	Virtual mass force, N
K_{pq}:	Interphase momentum co-efficient, Kg s^{-1}
p_s:	Solid pressure, Pa
$\bar{\bar{\tau}}_s$:	s^{th} phase stress-strain tensor, Pa
K_{ls}:	Fluid-solid exchange co-efficient, Kg s^{-1}

K_{pq}: Fluid-fluid exchange co-efficient, Kg s^{-1}

K_{ls}: Fluid-solid and solid-solid exchange coefficient, Kg s^{-1}

f: Drag function,

τ_p: Particulate relaxation time, s

d_p: Diameter of the bubbles of phase p, m

C: Drag co-efficient

Re : Reynolds number

ρ_{rp}: Mixture density of phase p and r, kg m^{-3}

μ_{rp}: Mixture viscosity of phase p and r, m s^{-1}

α_p: Volume fraction of phase p, m s^{-1}

μ_p: Viscosity of phase p, m s^{-1}

α_r: Volume fraction of phase r

μ_r: Viscosity of phase r, m s^{-1}

μ_l: Viscosity of liquid phase, m s^{-1}

τ_s: Particulate relaxation time, s

d_s : Diameter of the particles of phase s, m

α_l: Volume fraction of liquid phase

ρ_l: Density of liquid phase, kg m^{-3}

$\vec{v}_l$: Velocity of liquid phase, m s^{-1}

e_{ls}: Coefficient of restitution

$C_{fr,ls}$: Coefficient of friction between the l^{th} and s^{th}solid phase particles

d_l: Diameter of particle of solid l, m

$g_{0,ls}$: Radial distribution coefficient

e_{ls}: Co-efficient of restitution for particle collisions

$g_{0,ls}$: Radial distribution function

Abstract

The term 'fluidization' is usually associated with two or three phase systems, in which the solid particles are fluidized by a liquid or gas stream flowing in the direction opposite to that of gravity. Fluidization where the liquid is a continuous phase is commonly conducted with an upward flow of the liquid in liquid-solid systems or with an upward co-current flow of the gas and the liquid in three phase systems. Under these conditions, a bed of particles with a density greater than that of the liquid is fluidized with an upward flow of the liquid counter to the net gravitational force of the particles. Fluidization can be achieved by downward flow of the liquid when the particles are having lesser density as compared to the continuous liquid medium. This phenomenon is termed as inverse fluidization. The inverse fluidization system has gained significant importance during the last decade in the field of environmental, biochemical engineering, and oil–water separation. The minimum fluidization velocity is lower in this case. Also it takes lesser energy to pump a fluid to force the particles in this case. Hence viewing on a larger scale, at the industrial level, it can save a lot of energy. Such energy efficient processes are the need of today when energy crisis is at its peak. The application of inverse fluidization technique in biotechnology is one of the most important areas in bioreactor engineering. In this report various hydrodynamic characteristics of the inverse fluidized bed is studied based on literature and CFD is proposed to be applied on the system for further analysis.

Chapter 1

INTRODUCTION

Current worldwide commercial activities for the treatment of industrial effluents and the waste water from many industries like distillery and sugar industries make use of the inverse fluidization technique because of the simplicity of the process. It is easy to operate and has low process cost. It also has the added benefits of low energy consumption and high efficiency as compared to normal fluidization technique and other methods. Because of lots of unique advantages such as high contacting efficiency between different phases, high heat and mass transfer rate, low pressure drop and convenient scheme for continuous operation, three-phase (gas–liquid–solid) fluidized beds have been widely adopted as effective multiphase reactors and contactors in the fields of biochemical, bioprocess, food, environmental and petrochemical engineering and industries. However, in the biochemical, food and environmental processes, solid materials such as bio-media, food particles, and adsorbent or absorption media have been usually small, permeable and less dense. Those kinds of absorbent or porous substrate media, whose density is lower than that of continuous liquid medium, have been reasonably fluidized by means of downward flow of liquid medium. This leads to more mass transfer coefficient due to high gas hold up and long residence time.

Inverse fluidization can be achieved by a downward flow of continuous liquid phase counter to net buoyancy force of the particles of lower density. Even though a number of experimental works has been done on the various parameters and physical properties, the complex hydrodynamics of inverse fluidization was not understood well because of the multiple phase interactions leading to further complications. Therefore, it is the need of the hour to develop a computational model to simulate the three phase inverse fluidization.

1.1. ADVANTAGES OF INVERSE FLUIDIZATION

One of the main advantages of inverse fluidization is its high mass transfer rates. As the liquid is introduced counter currently to the gas phase, it applies a drag force on the gas bubbles. Because of this, the gas hold-up and the mean residence time are much higher than other fluidized bed configurations. Another big advantage is the low energy requirement

owing to the low fluid velocities making this fluidized bed more economical. This is because the fluidization is done along the direction of gravity. The low velocities also help in minimizing the solid attrition and reducing the erosion of vessel. As the bed is expanding downwards, the particles which settle at the bottom could easily be removed. In view of these unique advantages, inverse fluidized bed (IFB) is applied to treat wastewater from domestic and process industries [Fan, 1989, Calderon et al., 1998]. They provide an efficient control of biofilm thickness. Bed expansion results as the liquid and the produced biogas flows in opposite directions [Garcia-Calderon et al., 1998].

1.2. APPLICATION OF INVERSE FLUIDIZATION

In view of the many advantages of inverse fluidization, it is nowadays being extensively used in biochemical, food processing, environmental and petrochemical industries. It is applied to treat waste water from domestic and process industries [Fan, 1989, Calderon et al., 1998, Rajasimman and Karthikeyan, 2006]. In three phase inverse fluidization, the biofilm thickness can be controlled at a very narrow range. Because of this it could be used for biological aerobic waste water treatment [Nikolov and Karamanev,]. This is also applied as airlift bioreactors. A few application of anaerobic inverse fluidized bed was also reported [Spiess et al., 1991, Meraz et al., 1996].

1.3. IMPORTANCE OF CFD FOR INVERSE FLUIDIZATION

Many experimental works were done till now to study the hydrodynamics of inverse fluidization. We can obtain information about the structure of the flow in a fluidized bed in experimental studies. Although these techniques have proven to be of great importance, there are also limitations and a full picture of the flow field is often hard to obtain in this way. Computational Fluid Dynamics, commonly abbreviated as CFD, is a technique to model fluid flow using a computer simulation. Till now, no major CFD analysis has been done on inverse beds. Hence, it is required to do a simulation to understand the fluidization behaviour more clearly.

A chief advantage of CFD is that it is a very compelling, discreet, virtual modeling technique with powerful visualization capabilities, and one can evaluate the performance of wide range of system configurations on the computer without the time, expense, and disruption required to make actual changes onsite.

Some of the many advantages that made CFD widely popular are the following:

- Without modifying and/or installing actual systems, CFD can predict which design changes are most crucial to enhance performance.
- Unmatched insight into systems that may be difficult to prototype or test through experimentation.
- CFD provides exact and detailed information about various parameters. The advances in technology require broader and more detailed information about the flow within an occupied zone, and CFD meets this goal better than any other method, (i.e., theoretical or experimental methods).
- CFD costs much less than experiments because physical modifications are not necessary.
- The numerical schemes and methods upon which CFD is based are improving rapidly, so CFD results are increasingly reliable. CFD is a dependable tool for design and analyses.
- CFD simulations can be executed in a short period of time.

1.4. OBJECTIVE OF PRESENT WORK

- Theoretical analysis and CFD simulation of an inverse fluidized bed and prediction of its hydrodynamic properties.
- To investigate numerically the hydrodynamic behaviour of the inverse fluidized bed mainly the bed expansion or bed voidage, minimum fluidization velocity and bed voidage.

1.5. OUTLINE OF THE REPORT

Chapter 1 includes a complete introduction of the project work including definition, advantages, and application of inverse fluidized bed. Importance of CFD for inverse fluidization is also discussed in this section. The main objective of the project work has also been reported in this chapter.

Chapter 2 covers the literature survey done on the topic. It is comprised of the hydrodynamic studies done on three phase inverse fluidized bed. Computational studies carried out in the field of fluidization are also covered.

Chapter 3 includes the experimental setup and the methodology followed. This chapter describes in details about the setup, methods and procedure.

Chapter 4 comprises of the CFD simulation of the inverse three phase fluidized bed. The model and various governing equations involved are discussed in detail. This also describes the geometry, meshing and solution parameters and controls.

Chapter 5 consists of the results of the work and detailed discussion for the same. A comparative study of the simulation results is carried out with the experimental data as well as with the data available in literature.

Chapter 6 comprises of the overall conclusion and future scope of the project work.

Chapter 2

LITERATURE SURVEY

Fluidization is a process with which a bed of solid particles is made to behave like fluid. The remarkable behaviour shown by the solid in fluidized condition can be utilised to cross the obstacles which it otherwise encountered. In the conventional fluidized beds, whilst the fluidization occurs from bottom to top, in inverse fluidization, it occurs in downward direction. The process of inverse fluidization comes into picture when the system deals with low density particles. The particles float on top of the fluidizing media, rendering the conventional method impossible.

The three phase fluidized beds can be operated with downward flow of the liquid counter to the net upward buoyancy force on the particles. The gas flow is upward, counter to the liquid flow and bed expansion can be supported by the (downward) liquid phase and the (upward) gas bubbles (Fan et al., 1982; Hinhet al., 1992; Krishnaiaet al., 1993; Legileet al., 1988). If the density of the particles remains smaller than but close to that of the liquid, the fluidization can be achieved only with an upward gas flow (Roustanet al., 1995). These multiphase systems are often named as inverse turbulent systems. At low liquid or gas velocities, the particles form a buoyant packed bed at the top of the column supported by the mesh. As the liquid or gas velocity is increased, bottom layer of the particles just fluidizes and the rest remains in packed condition. With further increase in the velocity, more and more particles at the bottom of the packed bed are fluidized and the bed height increases. At one particular velocity, the entire bed is in fluidized condition. The velocity corresponding to this condition is termed as ‘minimum fluidization velocity’. Though the entire bed is fluidized, the concentration of solids is not uniform along the axis of the bed. With further increase in the velocity, the solid holdup becomes uniform throughout the bed. This velocity is termed uniform fluidization velocity (Krishna et al., 2007).

2.1. HYDRODYNAMIC STUDY OF INVERSE FLUIDIZED BED

Many researchers have reported on bed dynamics for inverse fluidization such as bed pressure drop, bed expansion, phase hold ups and minimum fluidization velocity. Some of the studies are reported below in Table 1:

Table 2.1.Hydrodynamic study on inverse fluidized bed

Researcher	Parameter studied
Fan et al. (1998)	bed porosity and gas holdup
Briens et al. (1999)	The effect of the inhibitors on the minimum fluidization velocity can be predicted from their effect on gas holdup
Han et al. (2002)	effect of the surface hydrophilicity on phase hold up, critical fluidization velocity,
Bandaru et al. (2007)	pressure drop, minimum liquid and gas fluidization velocities and phase holdups
Hamdad et al. (2007)	gas velocity, phase hold ups
Lee et al. (2007)	gas and liquid velocities, liquid viscosity and media particle kind
Myre et al. (2010)	Phase holdups and instantaneous heat transfer coefficients.

2.1.1. Flow patterns in inverse gas-liquid-solid fluidization

As per the flow patterns, there are four distinct regimes into which the fluidization phenomena can be categorized. These are fixed bed (with/without partial fluidization) with dispersed bubble regime, inverse bubbling fluidized bed regime, transition regime, and inverse slugging fluidized bed regime(Fan et. al., 1982).

At the low liquid and gas flow rates (point A in the Figure 1.), the drag force exerted by the liquid and the turbulence generated by the bubbles does not exceed the net buoyancy force of the particles. Thus, the bed remains in a packed bed state. When the gas flow rate increases to that close to the incipient fluidization conditions, the lower region of the bed begins to fluidize. As the gas flow rate further increases, the remaining packed portion progressively expands until the entire bed is fluidized. The bed under such a condition is in a state of incipient fluidization and is indicated by point B in the figure. Point B also corresponds to the break point on a curve in the plot of dynamic pressure gradient ($-\frac{dP}{dz}$) defined as the static

pressure gradient corrected for the static liquid head, versus V_i. In this plot, the dynamic pressure gradient increases as V_i, increases until a break point is reached beyond which the increase in V_i, would decrease the dynamic pressure gradient. The definition of incipient fluidization for inverse gas-liquid-solid fluidization described here which is based on the dynamic pressure gradient variation is similar to that for the liquid-solid fluidized bed. In the inverse bubbling fluidized bed regime (between points B and D), the bubble size is uniform and the bed is expanded downward uniformly. In this regime the bed would expand by an increase in either the gas or liquid flow rate. As the gas flow rate increases beyond point D, the transition regime is reached. In this regime, the coalescence of the bubbles occurs. The frequency of the coalescence and size of the coalesced bubble increases with the increase of the gas flow rate. Point F is the inception of the inverse slugging fluidized bed regime. In this regime, the bed of particles aggregatively moves up with the slug bubble and then slumps violently.

For each gas velocity the minimum liquid fluidization velocity corresponds to the velocity at which the pressure gradient within the bed is minimum (Ibrahim et al., 1996). Hence, the minimum liquid fluidization velocity is obtained from a plot of pressure gradient vs. liquid velocity at a constant gas velocity as shown in Fig. 2. Though the entire bed is fluidized, the concentration of solids is not uniform along the axis of the bed. High concentration of solids is observed near the liquid distributor (Ibrahim et al., 1996). For further increase in the velocity, the solid holdup becomes uniform throughout the bed. This velocity is termed uniform fluidization velocity.

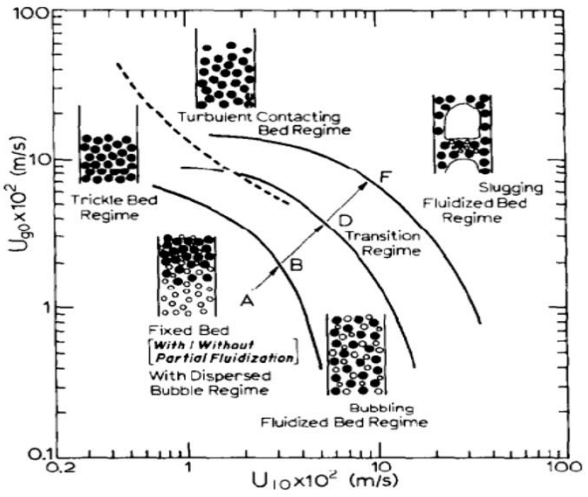

Figure 2.1 Flow regime diagram for inverse gas-liquid-solid fluidized bed (Fan 1982)

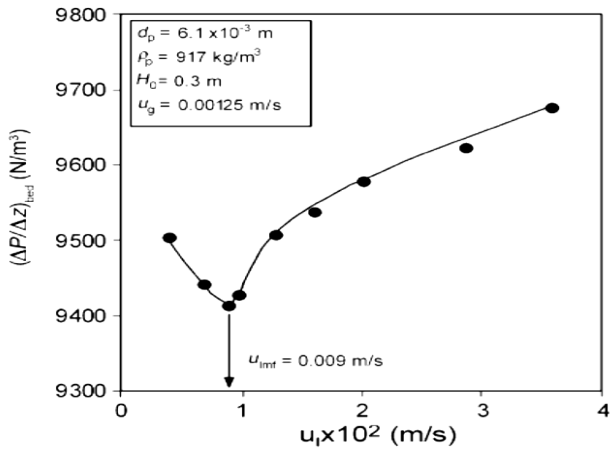

Figure 2.2 Determination of minimum fluidization velocity (Bandaru et al., 2007)

2.1.2. Bed Expansion

Figure 2 shows the variation of the bed height with the gas flow rate. As noted earlier, a slight bed expansion would occur when the bed is operated close to the incipient fluidization condition. Evidently, a slight increase in the height of the bed is observed between points A and B as shown in the figure. As the gas flow rate increases beyond point B, the bed expands until the bottom distributor plate is reached, which is represented by point C. Particles are fluidized in the entire column under this constrained condition until point E is reached. When the gas flow rate is slightly increased, the bed contracts sharply to a point F. When the gas flow rate is further increased, the bed increases again, but moderately. It is also noted that, for a given gas flow rate; the bed expands with an increase of the liquid flow rate under non-constrained fluidization condition. Extrapolation of the BC curve and the FE curve would intersect at a point which is defined as point D. The physical interpretation of point D is that should the column be extended, the maximum height of bed expansion would be that which corresponds to point D. In terms of the flow regimes defined in Fig. 1, the following regimes occur in order: fixed bed (with/without partial fluidization) with dispersed bubble regime from point A to B, inverse bubbling fluidized bed regime from point B to D, transition regime from point D to F, inverse slugging fluidized bed regime beyond point F. In addition, the constrained fluidized bed regime ranges from point C to E.

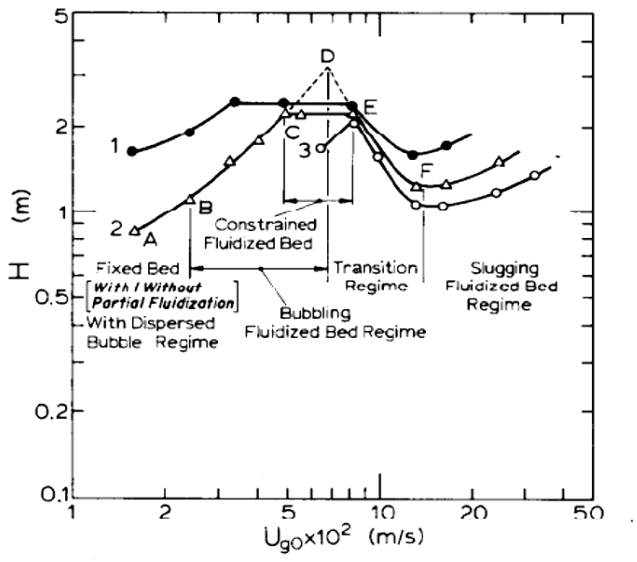

Figure 2.3 Variation of bed height with superficial gas velocity (Fan et al., 1982)

2.1.3. Pressure drop

The determination of pressure drop facilitates us to determine friction factor i.e. energy loss and conditions of stable flow regimes of inverse fluidised bed reactor for the given operation. As in classical fluidisation the pressure drop increases with increase in liquid flow rate till the condition of onset of fluidisation is reached which represents packed bed. On further increase the pressure drop remains almost constant as the resistance for the liquid decreases significantly. The pressure drop increases with increase in initial bed height (Bendict et al., 1998).

2.1.4. Minimum fluidization velocity

The bed height remains unaffected up to a certain liquid flow rate and thereafter varies linearly with flow rates for different initial heights and solid densities. With further increase in flow rate, a condition (net upward force = net downward force) is reached where the lowest layer of the particles just starts to get detached from the bed. The velocity corresponding to this flow rate is termed as minimum fluidisation velocity, U_{mf} and the condition is referred as on-set of fluidisation. With further increase in flow rate, more and more particles get detached from the packed bed, bed height increases linearly as the

downward force due to the liquid overcomes the upward buoyancy forces due to the low density particles.

2.1.5. Phase holdup

Gas hold-up

The gas hold-up ε_g is plotted against the superficial gas velocity U, as shown in Fig. 3. It is noted that in the inverse bubbling fluidizing bed regime the liquid flow rate has negligible effect on ε_g. In contrast, in the conventional co-current up-flow gas-liquid-solid fluidized bed using large particles, the gas hold-up decreases with an increase in the liquid flow rate. Furthermore, in the inverse slugging fluidized bed regime, the gas hold-up increases with an increase in the liquid flow rate. The gas hold-up increases with increase in gas velocity (Kim et al., 2007).

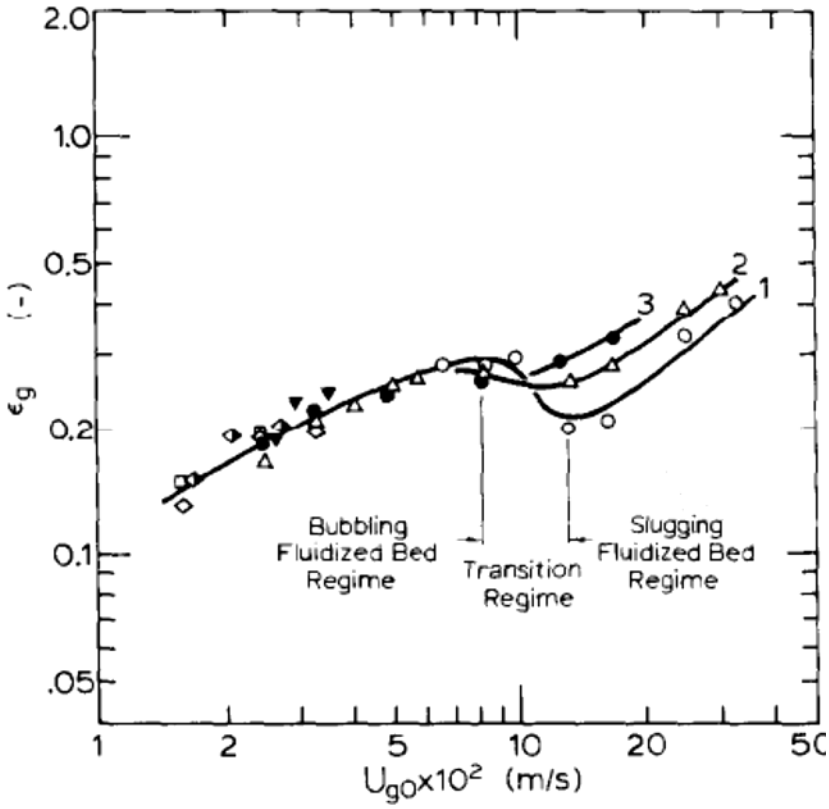

Figure 2.4 Variation of gas volume fraction with superficial gas velocity (Fan et al., 1982)

Liquid hold-up

In the fluidized bed region the liquid holdup increases with liquid velocity at constant gas velocity. The variation of liquid holdup with the variation of gas velocity was somewhat complicated. That is, in the relatively low range of liquid velocities, the liquid holdup increases with increasing gas velocity, whereas in the relatively high liquid velocity range, the value of the liquid holdup exhibits a local maximum with increasing gas velocity. The reason why the liquid holdup increases gradually with increasing gas velocity could be due to the fact that the bed can expand with increasing gas velocity in a given liquid velocity.

Solid hold-up

The solid holdup decreases generally with increasing gas or liquid velocity. The solid holdup in the beds of relatively-low-density particles exhibited a higher value than that in the beds of relatively-high-density particles. The particle concentration also has an effect on phase hold-ups. Solid hold-up increases naturally with solid loading, and decreases gas and liquid loading.

Studies (Han et al., 2003) also show that the surface properties of particles must also be considered in deciding phase holdups. When two particles have same densities but different surface properties it is always advisable to use the hydrophobic particles.

2.2. CFD MODELLING DONE ON CONVENTIONAL THREE PHASE FLUIDIZED BEDS

- Bahary et al. (1994) carried out CFD simulation on three-phase fluidized bed, where gas phase was particulate phase. A kinetic theory granular flow model was applied for solid phase. They took into consideration both symmetric and axisymmetric model and verified the different flow regimes in the fluidized bed by comparing with experimental data.
- Li et al. (1999) have studied three-phase fluidization with two dimensional simulation using Eulerian-Lagrangian model. The dispersed particle method (DPM) and the volume-of-fluid (VOF) method have also been used. Single bubble rising velocity in a liquid-solid fluidized bed and the bubble wake structure and bubble rise velocity in liquid and liquid-solid medium was investigated.
- A study was carried out on bubble column reactors by Joshi et al. (2001) using Euler-Lagrange approach. The effect of drag force, virtual mass force and lift force and

mechanism of the energy transfer from gas to liquid phase was explained. The effects of the superficial gas velocity, column diameter and bubble slip velocity on the flow pattern have been examined and compared with experimental velocity profiles.

- Matonis et al. (2002) used the Kinetic theory granular flow (KTGF) model for describing the particulate phase using multi-fluid Eulerian approach for slurry bubble column. The time averaged solid velocity, volume fraction profiles, shear Reynolds stress have been analysed and compared with experimental data.
- Feng et al. (2005) carried out 3-D, multi-fluid Eulerian analysis of three-phase bubble column. The liquid phase along with the solid phase considered as a pseudo-homogeneous phase in view of the ultrafine nanoparticles. The interface force model of drag, lift and virtual mass and k-ε model for turbulence have been taken. They reviewed the local time averaged liquid velocity and gas holdup profiles along the radial position.
- Zhang and Ahmadi (2005) have used 2-D, Eulerian-Lagrangian model for three-phase slurry reactor. The interactions between bubble-liquid and particle-liquid have been included. Particle-particle and bubble-bubble interactions have been accounted for by the hard sphere model approach. Transient characteristics of gas, liquid and particle phase flows in terms of flow structure, effect of bubble size on variation of flow patterns and instantaneous velocities had been studied.
- Panneerselvam et al. (2009) worked upon 3D, Eulerian multi-fluid approach for gas-liquid-solid fluidized bed. Kinetic theory granular flow (KTGF) model for describing the particulate phase and a k-ε based turbulence model for liquid phase turbulence had been used. The interphase momentum between two dispersed phases has been included.

Chapter 3

EXPERIMENTAL SET-UP

An inverse solid-liquid-gas fluidized bed was used to study the hydrodynamic behaviour. The inverse fluidized bed is operated in different modes. It can be operated with dispersed gas phase sent from the bottom of the column through the liquid phase which can be either in batch or continuous mode. In 3-phase IFB with liquid in batch mode, the solid particles are maintained in a fluidized condition by means of gas flow only with no net liquid flow. In the continuous mode of operation, there is a flow of both liquid and gas phase and both phases contribute to the downward fluidization of the particles.

3.1. Experimental set-up

The experimental setup is as shown in figure 1. The column is made of Perspex with a height of 1240 mm and a wall thickness of 3 mm and 100 mm internal diameter.

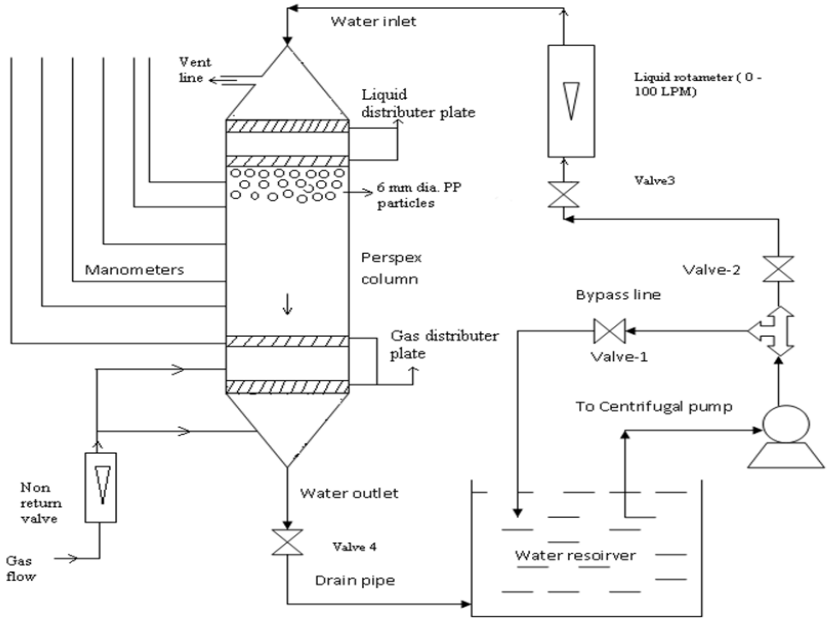

Figure 3.3 Schematic diagram of the experimental set-up.

The column consists of the following three sections:

Conical liquid distribution section: This section comprises of a cone with angle of 30º whose large base diameter is 10 cm and the smaller base diameter is 3 cm. At the top, an exit is provided for the inlet gas.

Test section: The test section is a column of height 100 cm and 10 cm diameter. Pressure tappings are provided at equal distance throughout the column. The pressure tappings are in turn connected with manometers.

Conical liquid discharge section: This section is geometrically similar to the upper liquid distribution section. It consists of an outlet for the water and at the bottom of the column another distributor is given to prevent the particles from escaping the bed. This also works as an air sparger. A non-returning control valve is there to let the air in.

The design of the conical liquid distributor was done in a manner so that proper liquid distribution could be ensured. The liquid was pumped to the top of the column and the flow rate was measured using calibrated rotameters (0 - 100 LPM). A control valve is also provided in the discharge line to adjust the flow rate. For the hydrodynamic study, water was used as the fluidizing liquid. The liquid discharge section is connected to a reservoir via a pipe so as to transfer the liquid to the tank.

3.2. Parts of Setup:

1. The fluidised bed consists of a Perspex column with a height of 1024 mm and a diameter of 100 mm. The thickness of the column is 3 mm.

2. To pump the water a Centrifugal Pump was used. (0.5 HP, 14 ft.)

3. Calibrated water Rotameter of capacity 0-100 LPM was used.

4. Calibrated air rotameter measuring flow rate (0-1000lph) was used.

5. Five manometers with standard length of 1.0 m wereused.

6. Syntax water reservoir - capacity: 1000 Litres.

8. Circular pitch distributor plates with different pitch diameters are used.

9. Two Conical heads with apex angle of 60^0 are used at the top and bottom of the column. (Inner base diameter = 100 mm, height = 30 cm).

3.3. Experimental procedure:

1. The two rotameters were calibrated by comparing the reading with the measured flow rate.
2. In a typical experiment, the column was loaded with solid particles of a particular size and density of the required bed height.

3. Water was supplied to the column at a known flow rate and the system was allowed to attain steady state by adjustment of inlet and discharge flow rate.

4. The manometers were filled with carbon tetrachloride and the pressure drop across the test section was noted from the manometers.

5. The water flow rate was increased gradually in steps until the bed was completely fluidized. These bed heights were measured by visual observation.

6. The minimum fluidization velocity was noted down.

Chapter 4

COMPUTATIONAL FLUID DYNAMICS

Computational fluid dynamics deals with the study of fluid flow problems by analysis using properly set algorithms. Computers are used to perform numerous calculations involved using software such as Fluent, CFX. Navier–Stokes equations form the fundamental basis of almost all CFD problems which define any single-phase fluid flow. These equations can be simplified by removing terms describing viscosity to yield the Euler equations. Further simplification, by removing terms describing vorticity yields the full potential equations. They can be linearized to yield the linearized potential equations. Even with simplified equations and high speed supercomputers, in many cases only approximate solutions can be achieved. More accurate codes are written that can accurately and quickly simulate even complex scenarios such as supersonic or turbulent flows.

Even though fluidization is a winning and effective technology having a wide range of applications, the design of fluidized beds is quite complex as their performance depends greatly upon a wide range of physical and operating variables. These variables include particle density, viscosity of the fluid, temperature, flow rates, pressure conditions, bed dimensions etc. For many years, the design of fluidized beds was solely based upon experimental correlations. Recently, as researchers have understood that the design equations can be analysed with respect to differential equations of momentum and continuity, the use of CFD increased rapidly.

It allows us to design and simulate any real systems without having to design it practically. CFD predicts performance before modifying or installing systems. The ability to simulate the flow behaviour of any new product or process improves the understanding of fluid behaviour and hence it reduces the time of prototype production and testing, leading to a successful glitch free design. Using CFD, we can build a computational model that represents a system or device that we want to study. A key advantage of CFD is that it is a very compelling, non-intrusive, virtual modelling technique with powerful visualization capabilities, and researchers can evaluate the performance of any practical system on the computer without the time, expense, and disruption required to make actual changes on-site. After our required design is built, we apply the fluid flow physics and chemistry to this virtual model and correspondingly the software will output a prediction of fluid dynamics and related physical

phenomena (Kumar, 2009). Once the simulation is done then various parameters like temperature, pressure, mass fraction etc. can be analysed.

4.1. COMPUTATIONAL FLUID DYNAMICS CODES

Fluid dynamic problems are handled by means of CFD in following three steps: pre-processing, solving and post-processing.

1) Pre-processing:

In this initial step all the necessary information which defines the problem is assigned by the user. This consists of geometry, the properties of the computational grid, various models to be used, the initial and boundary conditions, the number of Eulerian phases, the properties of the materials, the physical and chemical phenomena involved, the time step and the numerical schemes.

2) Solving:

The numerical scheme that most commercial CFD codes adopt is the finite volume method. The differential transport equations are integrated over each computational cell, and the Gauss and Leibnitz theorems are applied. A set of integral equations that express conservation laws on a control-volume basis is obtained. These equations are then converted into algebraic equations by using discretization techniques. At last, the set of algebraic equations is solved iteratively and the cell-centre values of the flow variables are calculated.

3) Post-processing:

In the final step the simulation results are analysed, diagrams and animations are created by using various graphics tools. The results of the simulation could thus be obtained in visually explaining contours and graphs.

4.2. LIMITATIONS OF CFD

- CFD solutions rely upon physical models of real world processes (e.g. turbulence, compressibility, chemistry, multiphase flow, etc.). The CFD solutions can only be as accurate as the physical models on which they are based.
- Solving equations on a computer invariably introduce numerical errors.
- As with physical models, the accuracy of the CFD solution is only as good as the initial/boundary conditions provided to the numerical model.

4.3. CFD APPROACHES IN MULTIPHASE FLOWS

4.3.1. The Euler-Lagrange Approach

The Lagrangian discrete phase models in FLUENT follow the Euler-Lagrange approach. The fluid phase is treated as a continuum by solving the time-averaged Navier-Stokes equations, while the dispersed phase is solved by tracking a large number of particles, bubbles, or droplets through the calculated flow field. The dispersed phase can exchange momentum, mass, and energy with the fluid phase. A fundamental assumption made in this model is that the dispersed second phase occupies a low volume fraction, even though high mass loading (m particles ≥ m fluid) 18 is acceptable. The particle or droplet trajectories are computed individually at specified intervals during the fluid phase calculation. This makes the model appropriate for the modelling of spray dryers, coal and liquid fuel combustion, and some particle-laden flows, but inappropriate for the modelling of liquid-liquid mixtures, fluidized beds, or any application where the volume fraction of the second phase is not negligible (Fluent, 2006).

4.3.2. The Euler-Euler Approach

In the Euler-Euler approach, the different phases are treated mathematically as interpenetrating continua. Since the volume of a phase cannot be occupied by the other phases, the concept of the phase volume fraction is introduced. These volume fractions are assumed to be continuous functions of space and time and their sum is equal to one. Conservation equations for each phase are derived to obtain a set of equations, which have similar structure for all phases. These equations are closed by providing constitutive relations that are obtained from empirical information, or, in the case of granular flows, by application of kinetic theory. In FLUENT, three different Euler-Euler multiphase models are available: the volume of fluid (VOF) model, the mixture model, and the Eulerian model (Fluent, 2006).

4.3.2.1.The VOF Model:

The VOF model is a surface tracking technique applied to a fixed Eulerian mesh. It is designed for two or more immiscible fluids where the position of the interface between the fluids is of interest. In the VOF model, a single set of momentum equations is shared by the fluids and the volume fraction of each of the fluids in each computational cell is tracked throughout the domain. The applications of VOF model include stratified flows, free surface flows, filling, sloshing, and the motion of large bubbles in a liquid, the motion of liquid after a dam break, the prediction of jet breakup (surface tension) and the steady or transient tracking of any liquid- gas interface.

4.3.2.2. The Mixture Model:

The mixture model is designed for two of more phases (fluid or particulate). As in the Eulerian model, the phases are treated as interpenetrating continua. The mixture model solves for the mixture momentum equation and prescribes relative velocities to describe the dispersed phase. Applications of the mixture model include particle-laden flows with low loading, bubbly flows, and sedimentation and cyclone separators. The mixture model can also be used without relative velocities for the dispersed phase to model homogenous multiphase flow.

4.3.2.3.The Eulerian Model

To change from a single-phase model, where a single set of conservation equations for momentum, continuity and (optionally) energy is solved, to a multiphase model, additional sets of conservation equations must be introduced. In the process of introducing additional sets of conservation equations, the original set must also be modified. The modifications involve, among other things, the introduction of the volume fractions for the multiple phases, as well as mechanisms for the exchange of momentum, heat, and mass between the phases.

The Eulerian model is the most complex of the multiphase models. It solves a set of n momentum and continuity equations for each phase. Couplings are achieved through the pressure and inter phase exchange coefficients. The manner in which this coupling is handled depends upon the type of phases involved; granular (fluid-solid) flows are handled differently than non-granular (fluid-fluid) flows. For granular flows, the properties are obtained from application of kinetic theory. Momentum exchange between the phases is also dependent upon the type of mixture being modelled. Applications of the Eulerian Multiphase Model include bubble columns, risers, particle suspension, and fluidized beds.

4.4.CONSERVATION EQUATIONS

The continuity equation for phase q is:

$$\frac{\partial}{\partial t}\left(\alpha_q \rho_q\right) + \nabla.\left(\alpha_q \rho_q \overrightarrow{v_q}\right) = \sum_1^n \dot{m}_{pq} \qquad (1)$$

Where $\overrightarrow{v_q}$ is the velocity of phase q and $\dot{m}_{pq}$ is the mass transfer from pth to q th phase.

From mass conservation we obtain, $\dot{m}_{pq} = -\dot{m}_{qp}$

And $\dot{m}_{pp}$ =0

The momentum balance for phase q yields

$$\frac{\partial}{\partial t}\left(\alpha_q \rho_q \overrightarrow{v_q}\right) + \nabla.\left(\alpha_q \rho_q \overrightarrow{v_q}\,\overrightarrow{v_q}\right) = -\alpha_q \nabla \mathrm{p} + \Delta.\overline{\overline{\tau_q}} + \alpha_q \rho_q g_q + \sum_1^n\left(\overrightarrow{R_{pq}} + \dot{m}_{pq}\overrightarrow{v_{pq}}\right) + \alpha_q \rho_q\left(\overrightarrow{F_q} + \overrightarrow{F_{lift,q}} + \overrightarrow{F_{mv,q}}\right) \quad (2)$$

$\tau_q$is the stress strain tensor

4.4.1. Interphase interactions.

The equations for fluid-fluid and granular multiphase flows, as solved by FLUENT, are presented here for the general case of a n-phase flow

$$\frac{\partial}{\partial t}\left(\alpha_q\right) + \nabla.\left(\alpha_q\,\overrightarrow{v_q}\right) = \frac{1}{\rho_q}\left(\sum_1^n \dot{m}_{pq} - \alpha_q \frac{d\rho_q}{dt}\right) \quad (3)$$

The solution of this equation for each secondary phase, along with the condition that the volume fractions sum to one, allows for the calculation of the primary-phase volume fraction. This treatment is common to fluid-fluid and granular flows.

For fluid-fluid flows, each secondary phase is assumed to form droplets or bubbles. This has an impact on how each of the fluids is assigned to a particular phase. For example, in flows where there are unequal amounts of two fluids, the predominant fluid should be modelled as the primary fluid, since the sparser fluid is more likely to form droplets or bubbles. The exchange coefficient for these types of bubbly, liquid-liquid or gas-liquid mixtures can be written in the following general form:

$$K_{pq} = \frac{\alpha_q \alpha_p \rho_p f}{\tau_p} \quad (4)$$

Where f is the drag function and τ_p is the particulate relaxation time.

$$\tau_p = \frac{\rho_p d_p^2}{18\,\mu_q} \quad (5)$$

where$d_p$is the diameter of the bubbles or droplets of phase***p*.** Nearly all definition of ***f***includes a drag co-efficient *(C_D*) that is based on the relative Reynolds number (*Re*). It is the drag function that differs among the exchange co-efficient models. For all these situations, K_{pq}should trend to zero.

In the present model we have used Schiller and Naumann model to define the drag function *f*.

$$f = \frac{C_D Re}{24} \tag{6}$$

Where $C_D = 24\,(1 + 0.15\,Re^{0.687})/\,Re \qquad Re \leq 1000$

$C_D = 0.44 \qquad Re \geq 1000$

and *Re*is the relative Reynolds number. The relative Reynolds number for the primary phase *q* and secondary phase is obtained from

$$Re = \frac{\rho_{rp}\,|\vec{v}_r - \vec{v}_p|\,d_{rp}}{\mu_{rp}} \tag{7}$$

where$\mu_{rp} = \alpha_p \mu_p + \alpha_r \mu_r$is the mixture viscosity of the phase*p* and *r*.

Nearly all definitions of f include a drag coefficient (C_D) that is based on the relative Reynolds number (Re). It is this drag function that differs among the exchange-coefficient models.

For all these situations, K_{pq}should tend to zero whenever the primary phase is not present within the domain. To enforce this, the drag function f is always multiplied by the volume fraction of the primary phase. The various fluid-fluid exchange models are Schiller-Naumann, Morsi-Alexander, Symmetric etc.

4.4.2. The fluid-solid exchange coefficient

$$K_{sl} = \frac{\alpha_s \rho_s f}{\tau_s} \tag{8}$$

Here, $\alpha_s$is defined differently for the different exchange-coefficient models and τ_s is the particulate relaxation time. where*f*is defined differently for the different exchange co-efficient model and τ_s**,** the particulate relaxation time.

$$\tau_s = \frac{\rho_s d_s^2}{18\,\mu_l} \tag{9}$$

where$d_s$is the diameter of the particles of phase *s*.All definition of *f* includes a drag function *(C_D)* that is based on the relative Reynolds number *(Re_s)*. It is this drag function that differs among the exchange co-efficient models.

In our present study, we have taken Gidaspow model, the combination of Wen and Yu model and the Ergun equation.

When $\alpha_l > 0.8$**,** the fluid solid exchange coefficient K_{sl} is of the following form:

$$K_{sl} = \frac{3}{4} C_D \frac{\alpha_s \alpha_l \rho_l |\vec{v}_s - \vec{v}_l|}{d_s} \alpha_l^{-2.65} \quad (10)$$

where$C_D = \frac{24}{\alpha_l Re_s} [\, 1 + 0.15(\alpha_l Re_s)^{0.687}\,]$ (11)

whereRe_s is defined as,

$$Re_s = \frac{\rho_l d_s |\vec{v}_s - \vec{v}_l|}{\mu_l} \quad (12)$$

*l*is the l^{th} fluid phase, *s* is for the s^{th} solid phase particles and d_s is the diameter of the s^{th} solid phase particles

when $\alpha_l \leq 0.8$,

$$K_{ls} = \frac{3(1+e_{ls})\left(\frac{\pi}{2} + C_{fr,ls}\frac{\pi^2}{8}\right).\alpha_s \rho_s \alpha_l \rho_l (d_l + d_s)^2 g_{0,ls} |\vec{v}_l - \vec{v}_s|}{2\pi(\rho_l d_l^3 + \rho_s d_s^3)} \quad (13)$$

where e_{ls} = the coefficient of restitution

$C_{fr,ls}$ = the coefficient of friction between thel^{th} ands^{th}solid phase particles.

d_l = diameter of the particle of solid*l*

$g_{0,ls}$ = the radial distribution coefficient.

4.4.3. Turbulence Models

To describe the effects of turbulent fluctuations of velocities and scalar quantities in a single phase, FLUENT uses various types of closure models. In comparison to single-phase flows, the number of terms to be modelled in the momentum equations in multiphase flows is large, and this makes the modelling of turbulence in multiphase simulations extremely complex. The choice of model depends on the importance of the secondary-phase turbulence in your application. There are three methods for modelling turbulence in multiphase flows within the context of the k-ε models. In addition, ANSYS FLUENT provides two turbulence options within the context of the Reynolds stress models (RSM). Three methods which FLUENT provides for modelling turbulence in multiphase flows are Mixture turbulence model (default), Dispersed turbulence model and Turbulence model for each phase. The RSM turbulence model options are mixture turbulence model (the default) and dispersed turbulence model.

4.5. CHOOSING A MULTIPHASE MODEL

The first step in solving any multiphase problem is to determine which of the region's best represent the flow. General guidelines provide some broad guidelines for determining the appropriate models for each regime, and detailed guidelines provide details about how to determine the degree of interface coupling for flows involving bubbles , droplets or particles , and the appropriate models for different amounts of coupling. In general, once that the flow regime is determined, the best representation for a multiphase system can be selected using appropriate model based on following guidelines. Additional details and guidelines for selecting the appropriate model for flows involving bubbles particles or droplets can be found. For bubble, droplet and particle-laden flows in which dispersed-phase volume fractions are less than or equal to 10% use the discrete phase model. For bubble, droplet and particle-laden flows in which the phases mix and / or dispersed phase volume fractions exceed 10% use either the mixture model. For slug flow, use the VOF model. For stratified / free-surface flows, use the VOF model. For pneumatic transport use the mixture model for homogenous flow or the Eulerian Model for granular flow. For fluidized bed, use the Eulerian Model for granular flow. For slurry flows and hydro transport, use Eulerian or Mixture model. For sedimentation, use Eulerian Model.

4.6.GEOMETRY AND MESH

A 2D geometry was made using FLUENT. As the set up requires multiple inlets and outlets, the whole set up was considered instead of just going for the bed geometry. The whole of the bed including the conical sections and the distributors were incorporated into the geometry. The conical section is of 0.18 m height, with base diameter 0.1 m and top diameter 0.03 m. The cylindrical test section is of height 1.24 m with diameter .1 m. The air inlet and outlets were of .01 m diameter. The water inlet and outlet measured .03 m in diameter. A separate zone is made to stop the solid entertainment at both the top and bottom of the bed.

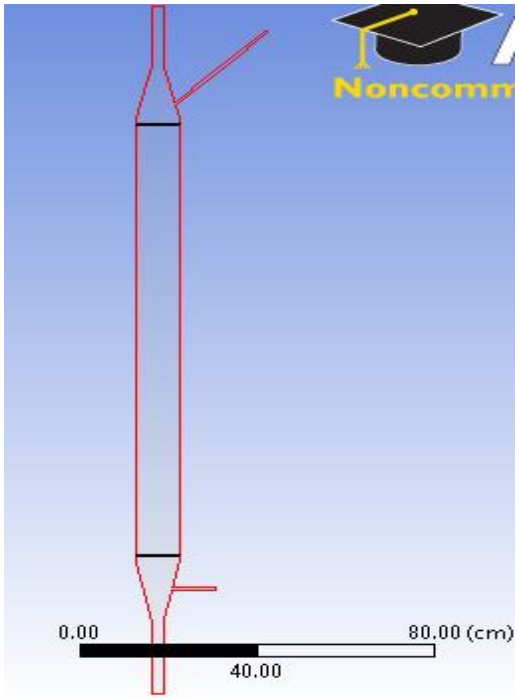

Figure 4.4 Geometry

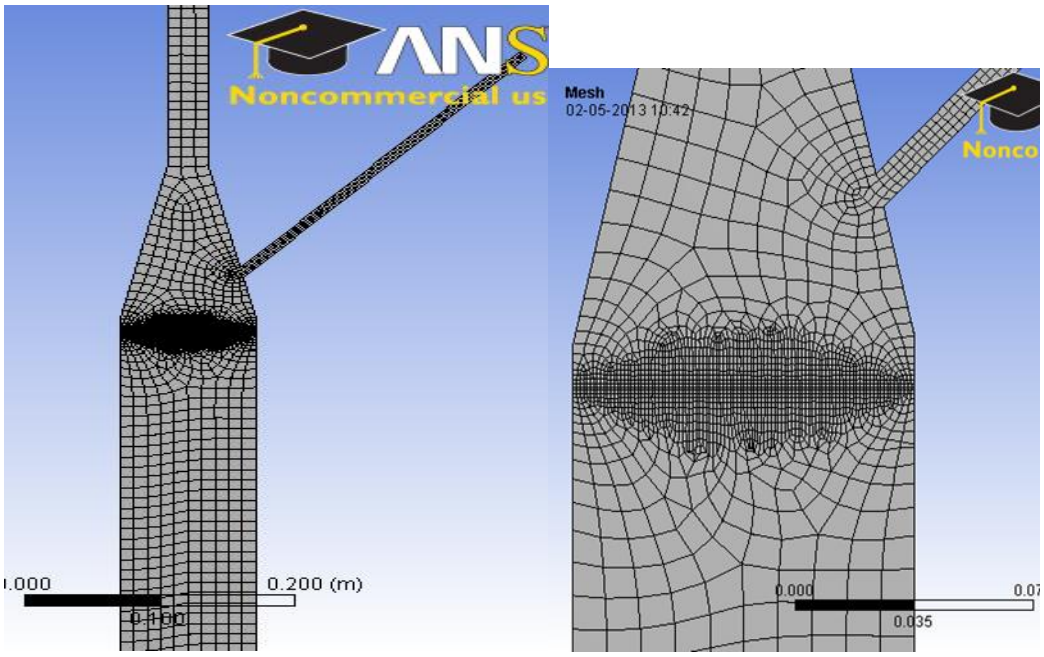

Figure 4.5 Meshing at the split-zone region

Mesh parameters

Table 4.1 Mesh parameters

Mesh type	Quadrilateral
Minimum element size	0.001 m
Maximum element size	0.01 m
Number of Nodes	6100
Number of Elements	5716

Selection of Models for Simulation

Governing and constitutive equations are implemented in the Multi Fluid Model of the package, based on the Eulerian-Eulerian description of the flow. Standard k-ε dispersed Eulerian multiphase model with standard wall functions were used. Water was taken as the continuous phase with the air and solid particles forming the secondary phases. The Schiller-Naumann model was used for the liquid-air inter-phase interactions, while the solid-fluid interactions were modelled using Gidaspow model.

4.7.BOUNDARY AND INITIAL CONDITIONS

The initial conditions for all simulation cases were set to the minimum fluidization condition with a bed volume fraction 0f 0.56 and bed height at minimum fluidization of 0.14 m. Air and water velocities with inlet air volume fractions obtained as fraction of air entering in a mixture of gas and liquid were the parameters used for boundary conditions. At the inlet the velocity inlet boundary condition with uniform superficial velocity of the gas and liquid phases were set. At the outlet the pressure outlet boundary condition was set.

Table 4.2 Phase parameters

Phases	Density (kg/m^3)	Viscosity (kg/m-s)
Water	998.2	0.001003
Air	1.225	$1.789*10^{-05}$
Polypropylene beads	910	0.001003

4.8.SOLUTION METHODS:

Table 4.3 Solution methods

Scheme	Multiphase coupled simple
Gradient	Least square cell based
Momentum	Second order upwind
Volume fraction	First order upwind
Turbulent kinetic energy	First order upwind
Turbulent dissipation rate	First order upwind
Transient formulation	First order implicit

Chapter 5

RESULTS

The gas-solid-liquid fluidized bed has been simulated using commercial CFD software package FLUENT 13.0.0. The results obtained through simulation are studied here. The hydrodynamic behaviour shown by the inverse fluidized bed analyses in this chapter.

5.1 CONTOURS OF VOLUME FRACTION OF SOLIDS

The simulation has been done for static bed height of 0.3 m with polypropylene particles of diameter 0.005 m. The results obtained have been presented graphically in this section.

Contours of volume fraction of bed with respect to time of fluidization are shown in the figure. The bed could be seen expanding with the passage of time. Initially, the particles at the bottom moves downward. With the passage of time the whole of the bed is agitated and eventually starts moving downwards. The static bed height at time 0 sec was 14 cm. After about 24 sec it was observed that the bed profile remained almost same. This is because the system attained a steady state at 24 seconds and further simulation had no significant effect on it. At about 15 seconds, it could be seen that a portion of the bed at the bottom separates out from the core body of the fluidized bed. This occurrence is explained by the phenomena of slugging. The fluctuations in velocity and the repulsive force between the particles are responsible for this behaviour. This happens when large air bubbles are formed which are greater than about one-third of the vessel diameter. This leads to pressure fluctuations and hence should be avoided when dealing with larger units.

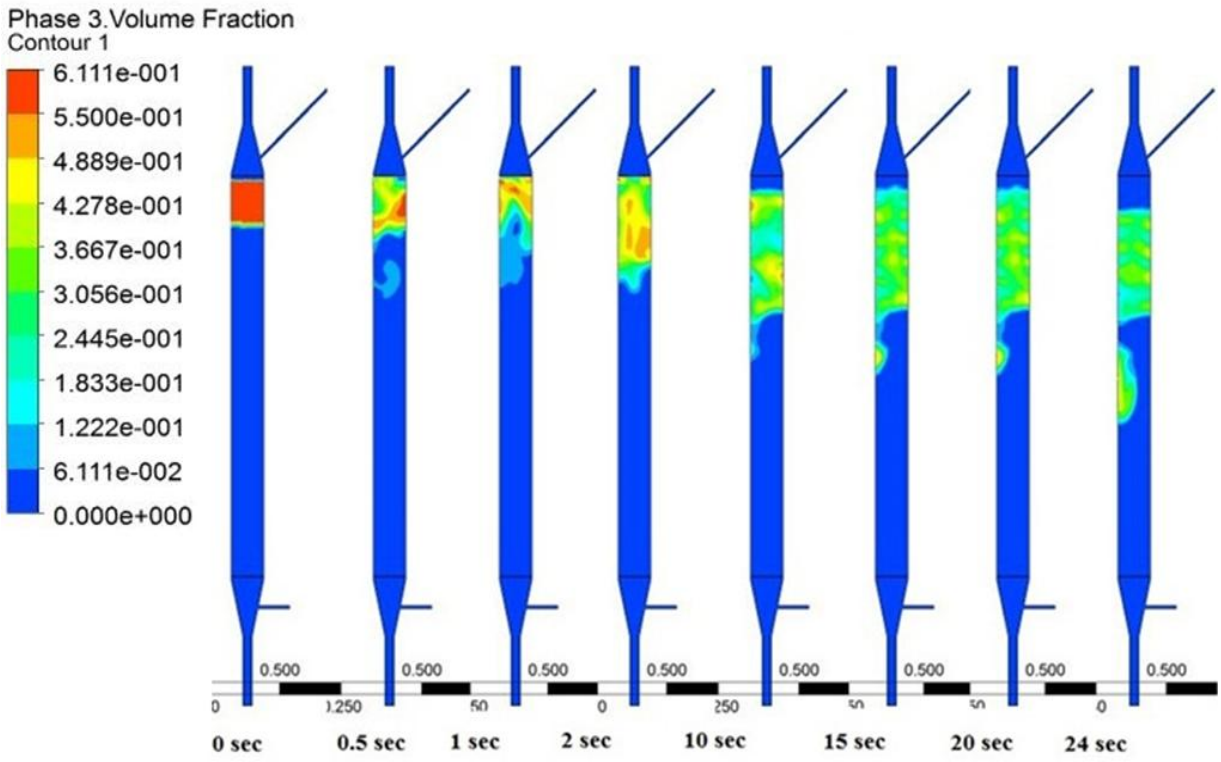

Figure 5.1 Contours of solid volume fraction at varying time intervals

5.2 PHASE DYNAMICS

Solid, liquid and gas phase dynamics has been represented in the form of contours, vectors and XY plots. Figure 7 shows the contours of volume fractions of solid, liquid and gas in the column obtained at a water velocity of 0.08 m/s and air velocity of 0.03m/s for static bed height 15 cm and polypropylene beads of diameter 5 mm after the quasi steady state is achieved. The contours for beads illustrates that bed is in fluidized condition. The contours of water illustrate that the volume fraction of water (liquid holdup) is less in the fluidized part of the column compared to remaining part. Similar is the case with air. The greater volume fraction of air is observed in the fluidized region than the region below the bed. This is because the air bubbles remain entrapped in the fluidized bed region for a higher residence time.

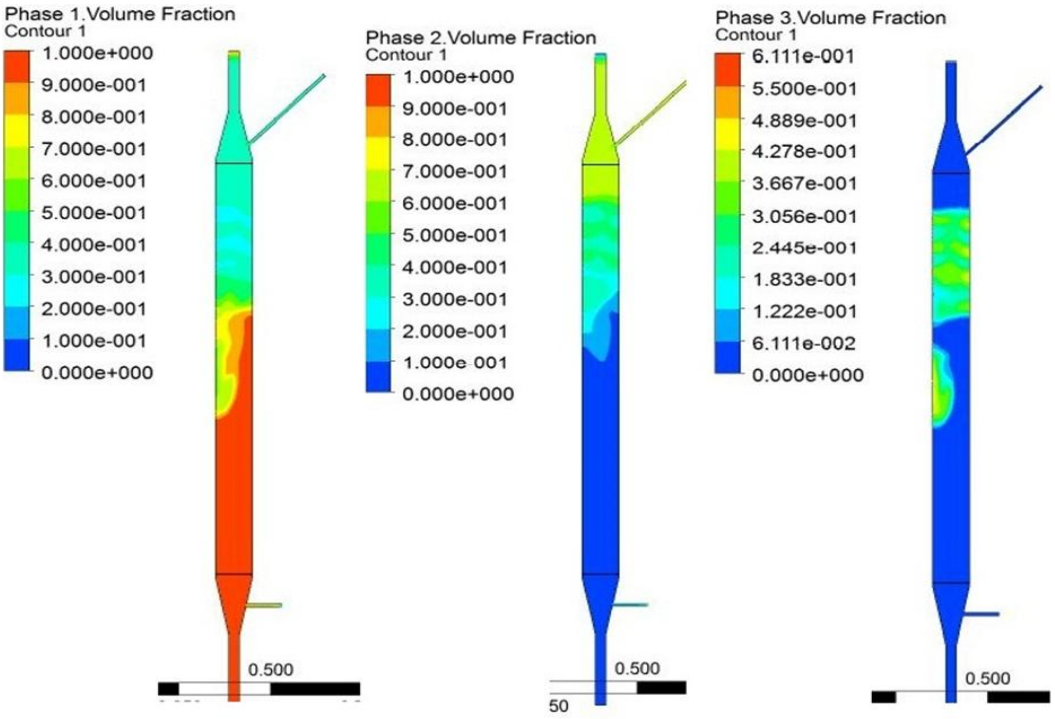

Figure 5.2 Contours of volume fraction of solid,liquid and air

5.3 VELOCITY VECTOR OF SOLID AND FLUID PHASES

Vectors of velocity magnitude of polypropylene beads, water and air in the column obtained at an inlet water velocity of 0.08 m/s and inlet air velocity of 0.03 m/s for static bed height 15 cm and polypropylene beads of diameter 5 mm after the quasi steady state is achieved are shown in figures 8-12. These vectors show the velocity magnitude with direction and thus helpful in determining flow patterns in fluidized beds. The velocity vector of water in the column as can be seen in figures 8 and 9 shows always a downward trend. The velocity decreases as it approaches the bed and inside the bed the velocity is very less. This is because less space is available for water to flow. As water leaves the bed and approaches towards the outlet again an increase in velocity can be seen.

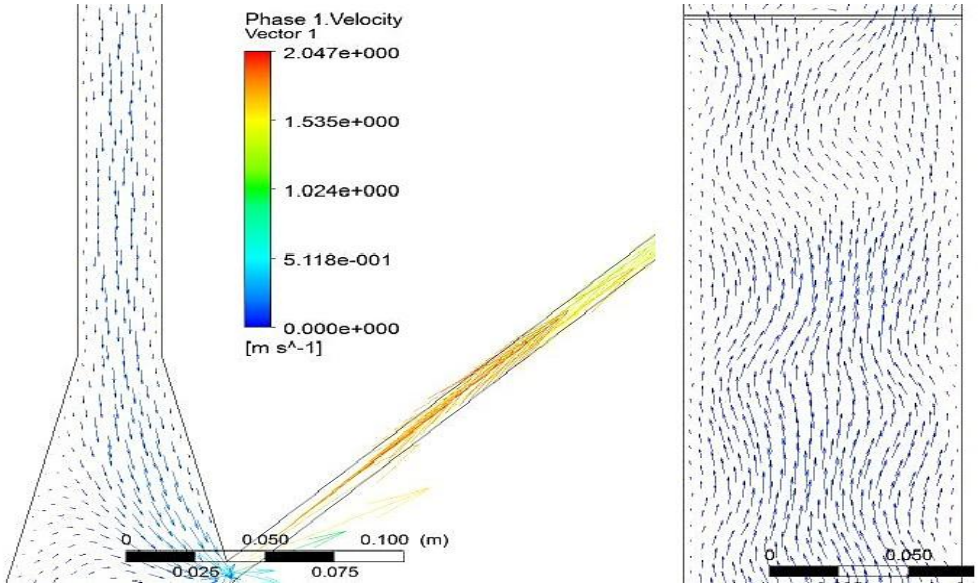

Figure 5.3 velocity vector of liquid phase

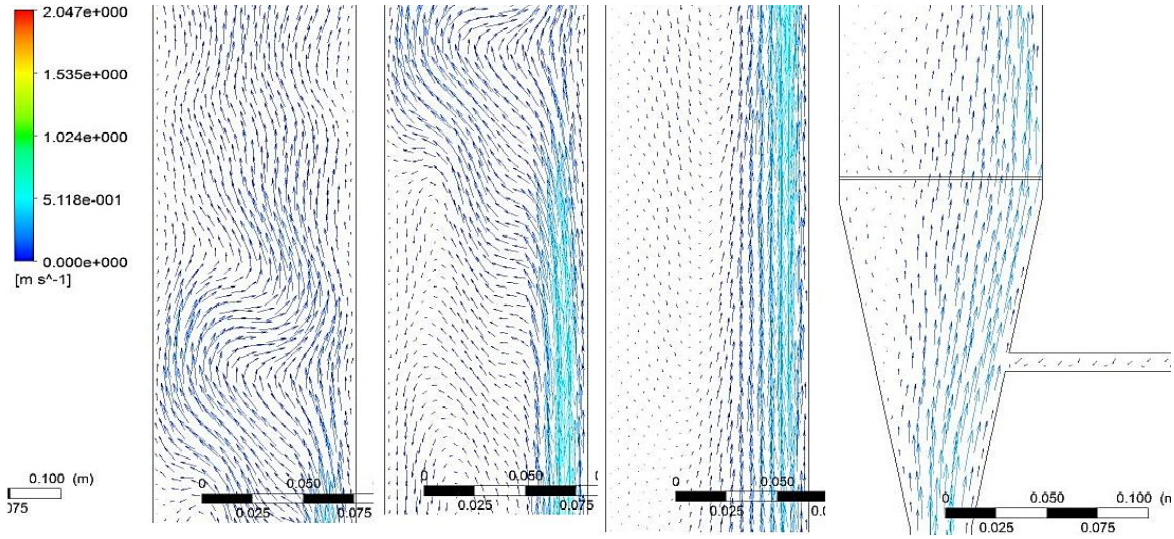

Figure 5.4 velocity vectors of liquid phase at different sections

The velocity of the air is very small in fluidized portion of the column compared to that in the remaining part of the column. This is because of the very small volume fraction of air compared to polypropylene beads and water. This may also happen that the solids block the air bubbles thereby lowering its velocity. In the upper section of the column; water, whose velocity is high carries air bubbles, so the velocity of air bubbles reduces.

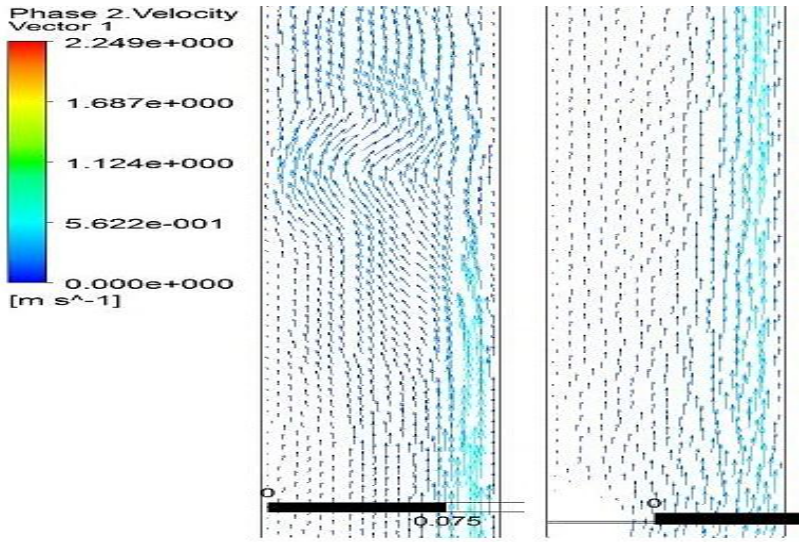

(a)

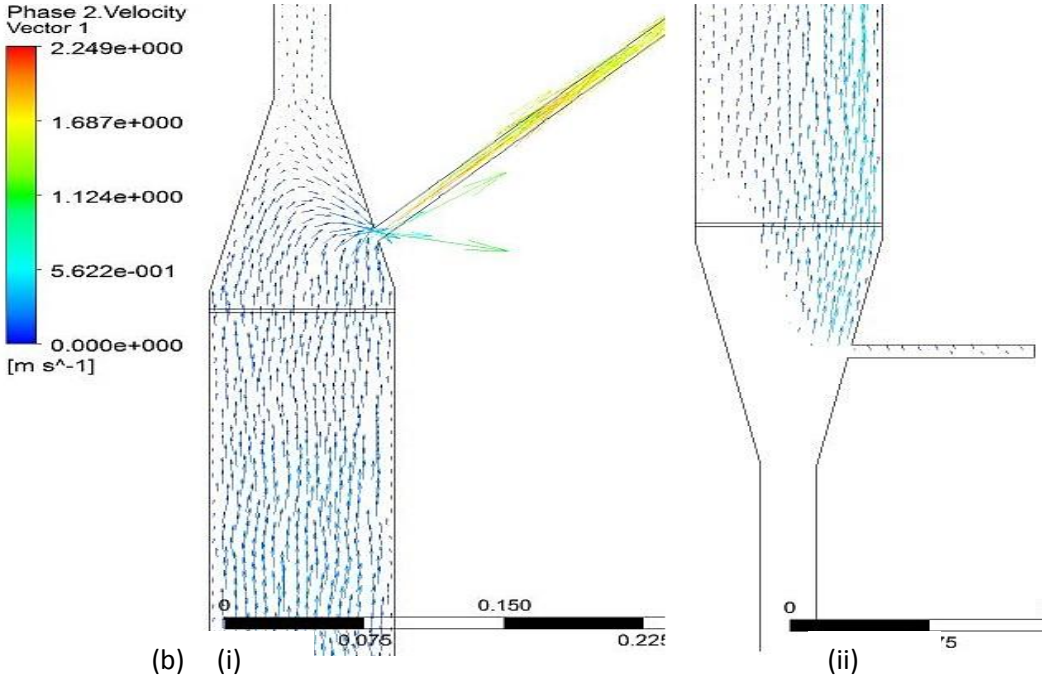

(b) (i) (ii)

Figure 5.5 velocity vector of air (a) at the middle section of the bed (b) at the top (i) and bottom (ii) conical sections.

The solid, liquid and gas velocity vectors varying radially at different bed heights are shown in fugures 5.6 – 5.8. All these are at for 5 mm diameter beads at liquid velocity of 0.08 m/s and gas velocity of 0.02 m/s. Fig. 5.6 shows the velocity vector of solid particles of diameter 5 mm at inlet liquid velocity 0.08 m/s and gas velocity 0.02 m/s. The negative sign of axial velocity is because the solids are moving in negative y direction. It is seen from the figure that the solid particle flows downward in the central region of the fluidized section. In the

lower section lessmovement of solid particles observed. Solid particles axial velocity is more in the central region of the fluidized bed and zero near to the wall. The axial velocity is seen to be maximum at a bed height of 1.15 m and 0 at 0.1 m, as the solid particles are negligible in that region.

The maximum liquid velocity is 0.48 m/s seen at a height of 0.45 m. the liquid velocity is seen to be more nearby the walls than at the centre. Also it could be seen that flow is in upward direction at the walls while at the centre the majority is flowing in downward direction.

From figure 5.7, from the variation of axial gas velocity along the radius, it could be seen that the gas velocity is uniform along the radius except at .75 m and 0.45 m. this shows that at the inlet and outlet and nearby the fluidized region the gas velocity is almost constant throughout the radius. However, at the middle regions, the gas velocity is seen to be varying radially.

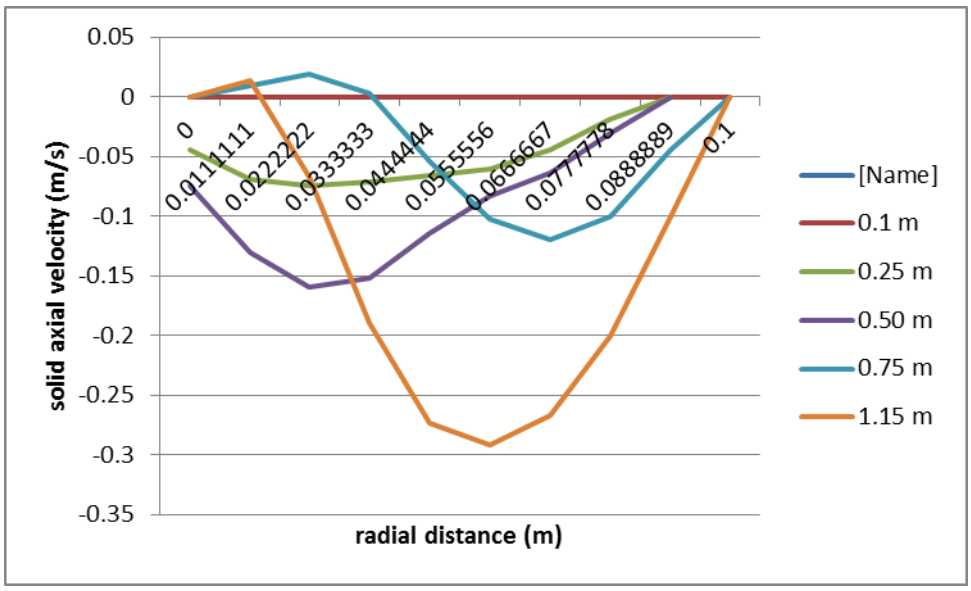

Figure 5.6 Variation of solid axial velocity with radial distance at 0.07 m/s liquid velocity and 0.02 m/s gas velocity

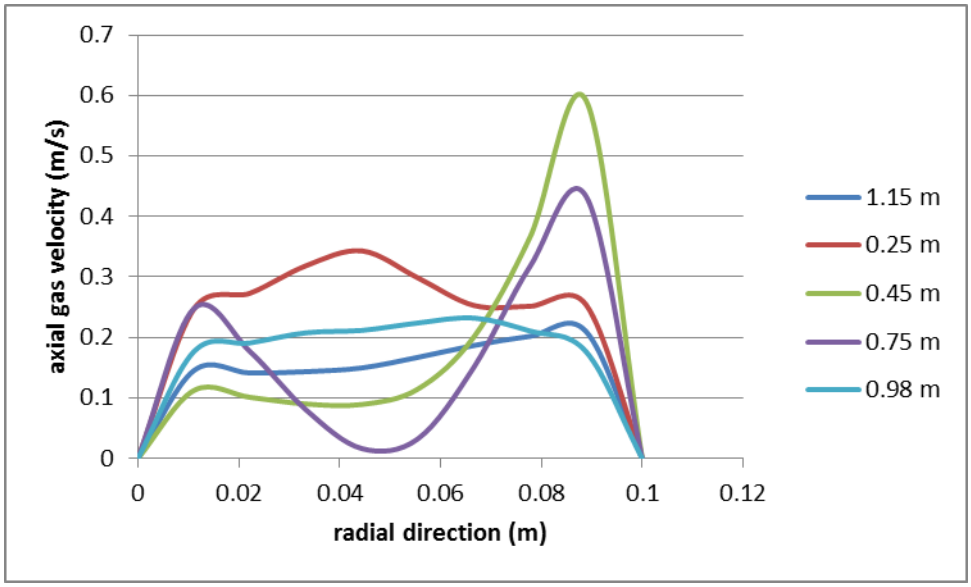

Figure 5.7 Axial gas velocity with radial direction at different bed heights for 0.07 m/s liquid velocity and 0.02 m/s gas velocity

Figure 5.8 depicts the variation of liquid velocity in radial direction at different bed heights. The profile is seen to be almost same at all bed heights. Near to the fluidized bed region, which is at a height of 0.98m and 1.15 m, the liquid velocity does not vary much radially. However, at other bed heights there is a fluctuation in radial distribution of velocity.

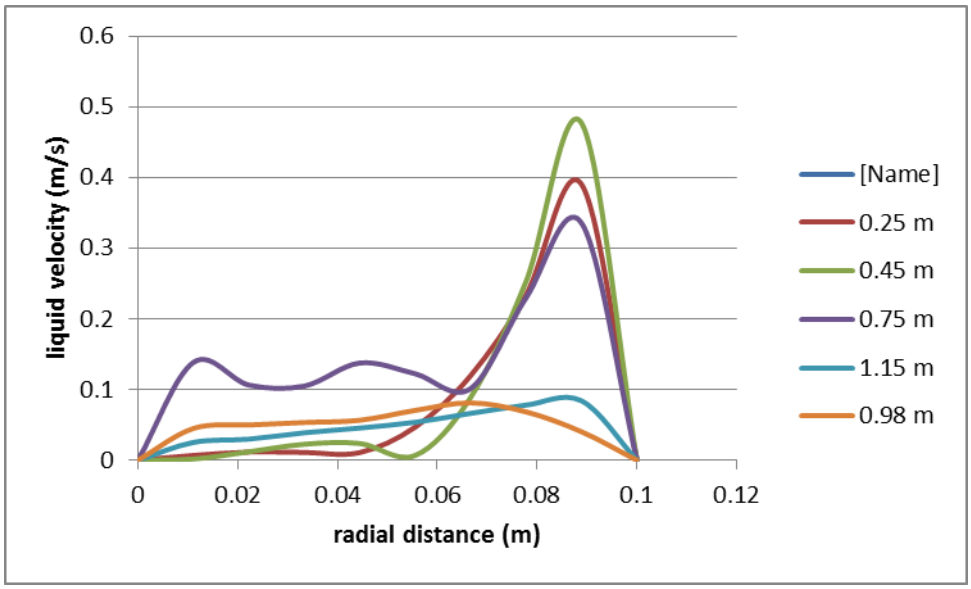

Figure 5.8 Variation of liquid velocity in radial direction

Figures 5.9 and 5.10 shows the axial gas and liquid velocity variations at a particular bed height respectively. At lower gas velocities, the axial velocity is not uniform along the radius. However, at higher gas velocities, the axial gas velocity is seen to be acting at same magnitude throughout the radial direction.

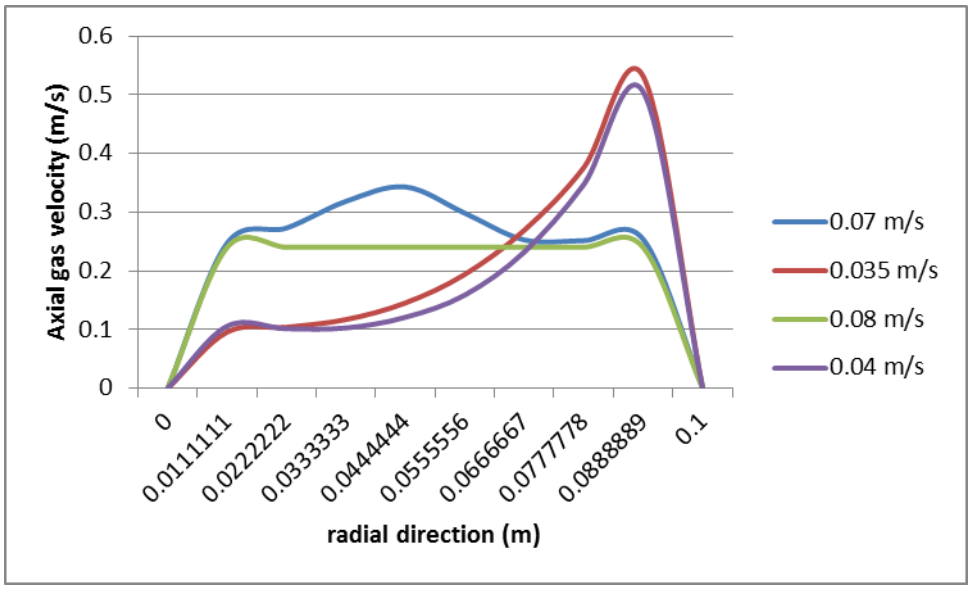

Figure 5.9 Variation of axial gas velocity in radial direction for 0.25 m bed height

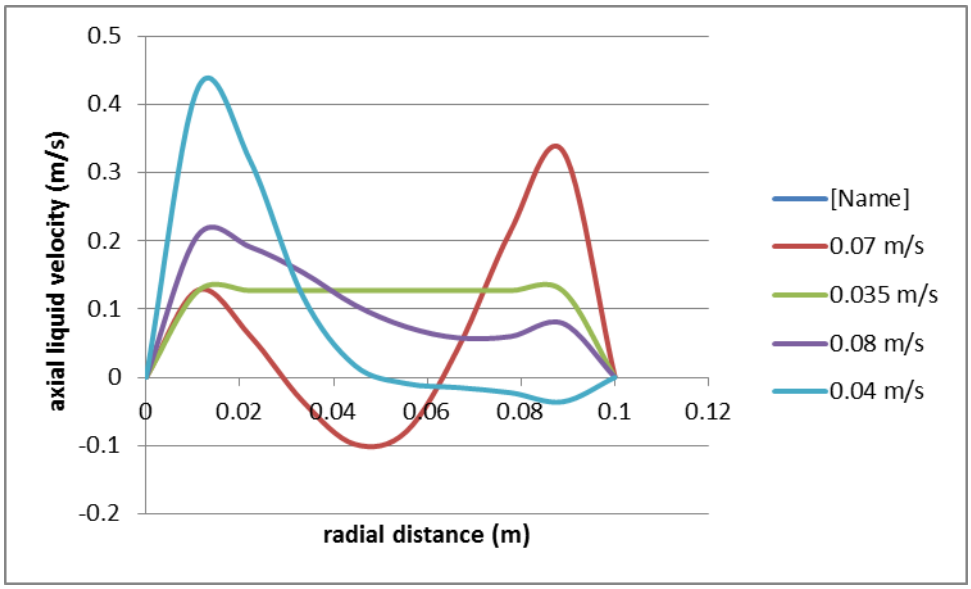

Figure 5.10 Variation of liquid axial velocity at a height of 0.75 m

The velocity of all the three phases is plotted aginst the bed height as shown in figure 5.11. the velocities of all the three phases are fluctuating in the fluidized region. The maximum gas velocity is 0.25 m/s and maximum liquid velocity is 0.15 m/s.

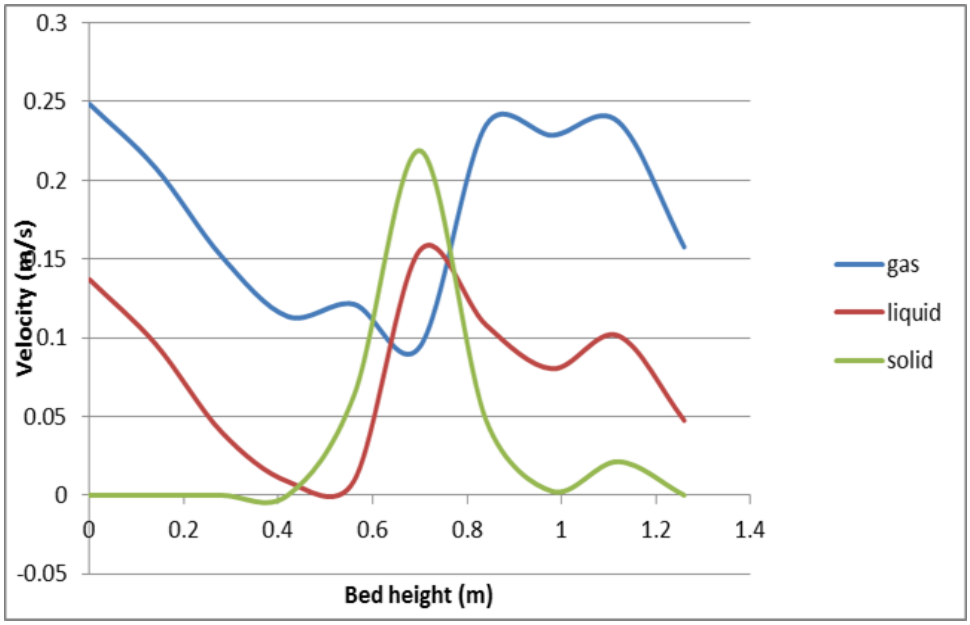

Figure5.11 Gas, liquid and solid velocities along the bed height at 0.07 m/s liquid velocity and 0.02 m/s gas velocity

5.4. BED EXPANSION

The following figure is the X-Y plot of the solid volume fraction with respect to axial direction along the bed. The expanded bed height is 75 cm as can be seen from the figure. The bed stars to expand only if the flow velocity is above minimum fluidization velocity. A higher excess velocity leads to higher expansion. Excess velocity is the difference in velocity between the minimum fluidization velocity and the superficial gas velocity.

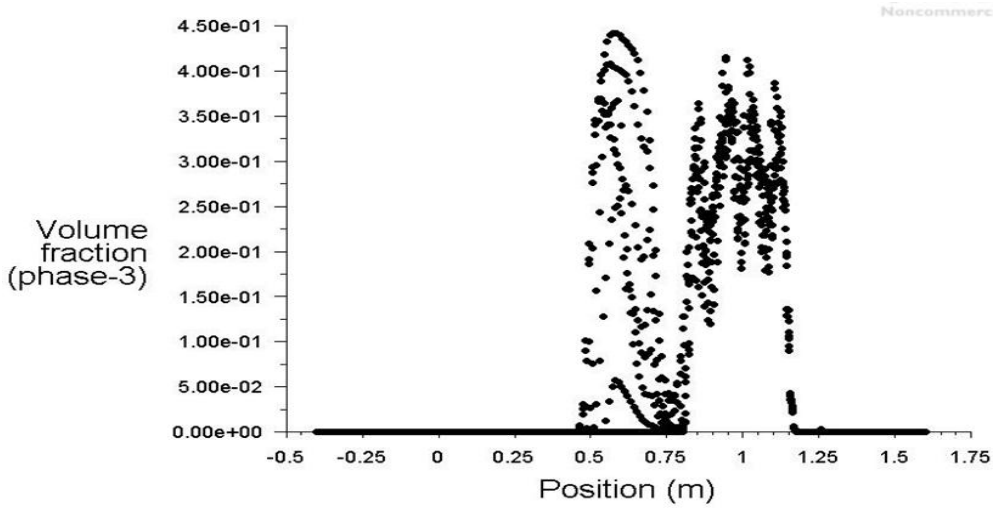

Figure 5.12 Variation of solid volume fraction along the bed in axial direction

5.5. PHASE HOLD-UP

The variation of gas-hold up at different bed height is as in figure 5.13. The variation is analysed radially. The gas hold up seems to be more in the upper section of the bed where the fluidized bed is formed. This is because the gas escapes from the lower sections to the upper bed and is trapped there. At each bed height, it could be seen that there is uniform gas distribution except at the region close to the air inlets. The gas seems to be evenly distributed within the expanded bed region.

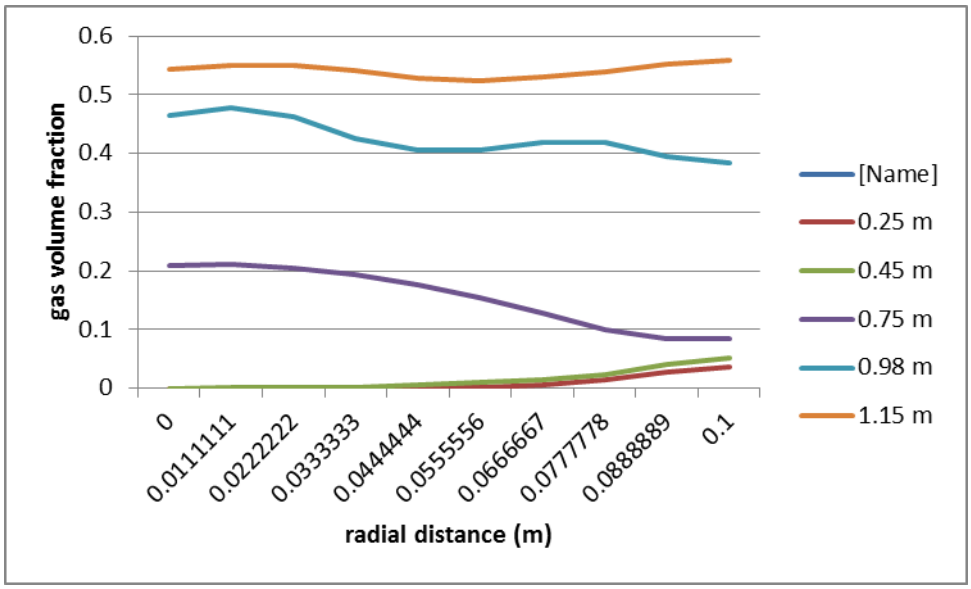

Figure 5.13 Variation of Gas hold-up with radial direction at different bed heights

Liquid velocity does not seem to affect gas hold-up much as can be seen from figure 5.14. Here the maximum volume fraction in the bed is 0.62 at a bed height of 1.25 m. The gas volume fraction is more at the upper portion of the bed where fluidized bed is present. In the remaining section, the volume fraction of air is seen to be negligible.

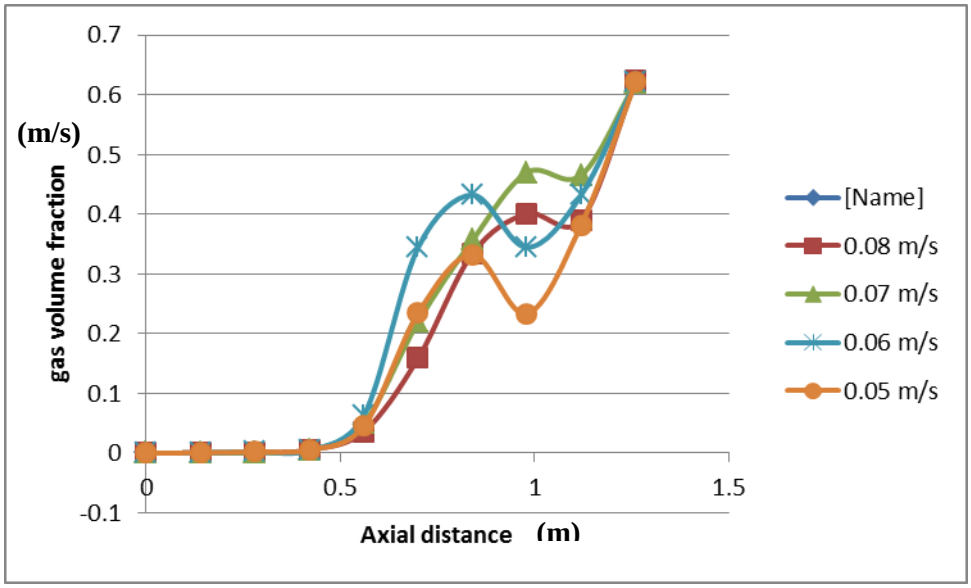

Figure 5.14 Variation of gas hold-up with increasing liquid velocity along axial direction

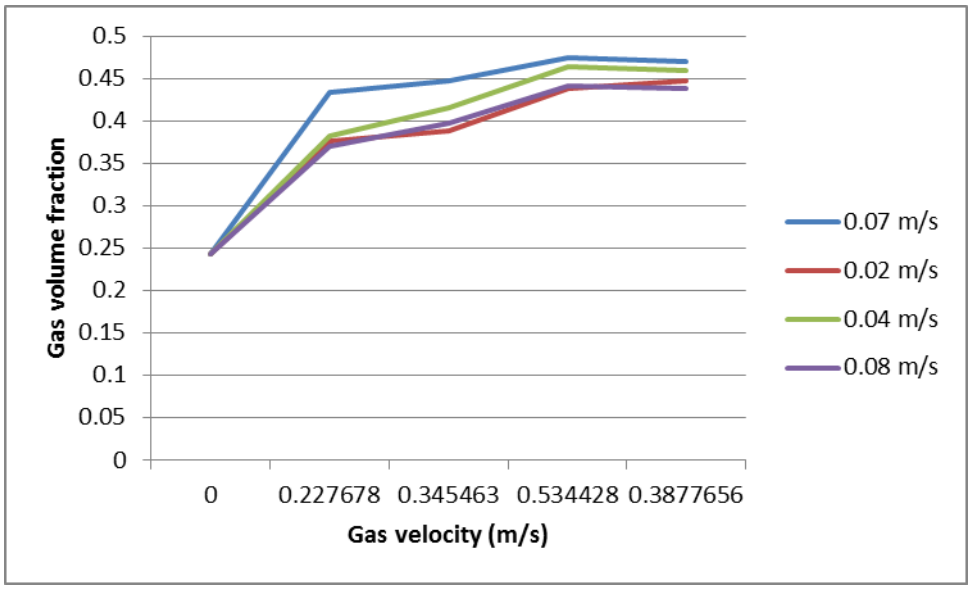

Figure 5.15 Variation of gas volume fraction with variation in gas velocity

5.6. PRESSURE DROP

The contour plot of static pressure at 0.08 m/s liquid velocity and 0.02 m/s gas velocity is as shown in figure 5.16 the pressure is seen to be decreasing as we move from top to bottom.

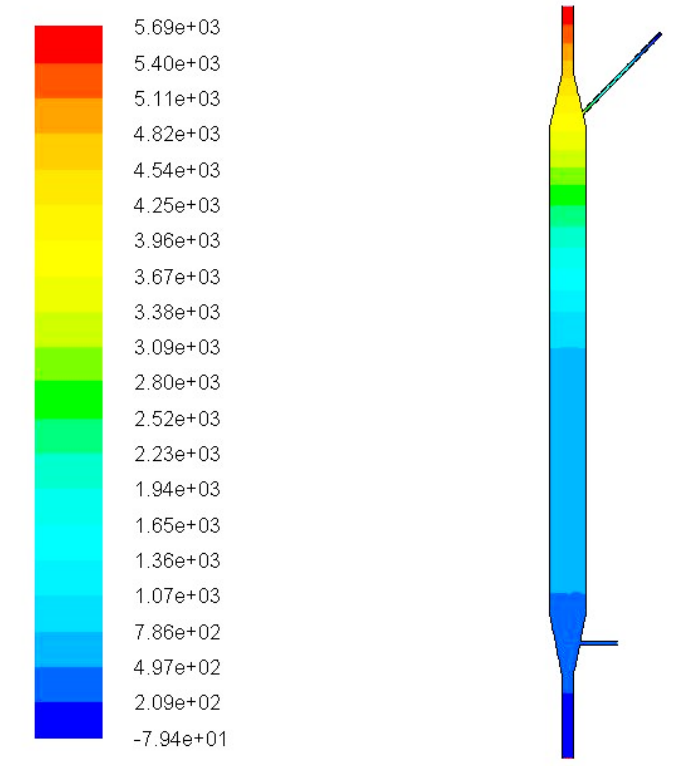

Figure 5.16 Contour of static pressure

Chapter 6

CONCLUSION

CFD simulation of hydrodynamics of inverse fluidized bed has been carried out for different operating conditions by employing the Eulerian-Eulerian granular multiphase approach. CFD simulation results have shown good agreement with available data for solid phase hydrodynamics in term of expanded bed height of the present experimental findings and liquid phase hydrodynamics in terms of phase velocities. The distribution of volume fraction of all the three phases inside fluidized section of the fluidized bed model explains the phenomena of inverse fluidization. The behaviour is in accordance to the explanation found in literature and experimental observation. The bed expansion behaviour with variation in liquid velocity obtained from CFD simulation to some extent has validated the experimental findings. Experimental result has shown an increase in bed expansion with liquid velocity, on the other hand CFD simulation has also shown slight increase in bed expansion. The bed pressure drop obtained from CFD simulation agree well with the experimental values. The good agreement between the values obtained from CFD simulation and experimental ones for the range of the present operating variables justify that the Eulerian-Eulerian multi-phase granular flow approach is capable to predict the overall performance of liquid–solid fluidized bed.

Some specific conclusions as described below can also be drawn with respect to the present work .

- It is observed from the contour plot of the simulation that steady state for inverse fluidization is attained at 24 seconds.
- Contours of liquid phase illustrates that the volume fraction of liquid is less in the fluidized zone.
- A greater volume fraction of air is seen near the fluidized bed region as the air bubbles get entrapped here.
- Velocity of the liquid phase decreases as it approaches the bed and inside the bed, velocity is very less as less space is available for water to flow. As water leaves the bed and approaches towards the outlet, again an increase in velocity is seen.

- Pressure drop increases and then attains a constant value suggesting no further increase in energy requirement after attaining steady state.
- Gas volume fraction is observed to be increasing for lower gas velocities. However with further increase in gas velocity, gas hold up remains constant. This is desirable as more surfaces is available for better contact.
- Solid axial velocity is found to be optimum at 1.15 m as the velocity is maximum at the centre for this height.
- Axial liquid velocity is almost uniform along the radius. Fluctuations could be seen, however, for a height of 0.45 m and 0.75 m.
- Liquid velocity does not vary much radially. However, at other bed heights, there is fluctuation in radial distribution of velocity.

The present work corresponds for a lab scale unit but it can also be applied for large scale applications. CFD analysis can be done on other applications of inverse fluidization which handles fluids like wastewater/other industrial effluents.

With the help of CFD studies for the Inverse Fluidized bed, proper design of a Bio-reactor can be made for optimizing the process.

Computational study of the system is more economical and less time consuming when we are dealing with large scale applications. Hence a hydrodynamic study of the system gives a full picture of the system behaviour at the same time saving time as well as resources.

FUTURE WORK

- CFD studies can be carried out for the effect of bubble size on hydrodynamics of fluidized bed for low density material.
- CFD studies can also be carried out for mass transfer and heat transfer operations in inverse fluidized bed.
- CFD studies can also be carried out for the hydrodynamics of 3D inverse fluidized bed.

REFERENCES

Arnaiz , C., Buffiere , P., Lebrato , J., and Moletta, R. (2007), "The effect of transient changes inorganic load on the performance of an anaerobic inverse turbulent bed reactor", Chemical Engineering and Processing, 46, 1349–1356.

Bandaru K., Murthy D. V. S., Krishnaiah K.(2007), "Some hydrodynamic aspects of 3-phase inverse fluidized bed", China Particuology, 5, 351-356.

Benedict and Moletta (1999), "Some hydrodynamic characteristics of inverse three fluidized bed reactors", Chemical Engineering Science, 54, 1233-1242.

Briens, C. L., Ibrahim, Y. A. A., Margaritis, A., and Bergougnou, M. A.(1999), "Effect of coalescence inhibitors on the performance of 3-phase inverse fluidized-bed columns", Chemical Engineering Science, 54,

Chen, C., Fan, L.S., (2004),"Discrete Simulation of Gas-Liquid Bubble Columns and Gas-Liquid-Solid Fluidized Beds."AIChE Journal 50, 288 -301.

Comte, M. P., Bastoul, D., Hebrard, G., Roustan, M. and Lazarova, V.(1997), "Hydrodynamics of a three-phase fluidized bed the inverse turbulent bed, chemical engineering science",52, 3971-3977.

Fan, L., Katsuhiko, M. and Chern, S (1982).,"Some remarks on hydrodynamics of inverse gasliquid- solid fluidization", Chemical Engineering science, 31,1570-1572.

Fan, L., Katsuhiko, M. and Chern, S.(1982), "Hydrodynamic Characteristics of Inverse Fluidization in Liquid-Solid and Gas-Liquid-Solid Systems", The Chemical Engineering Journal, 24, 143-150.

Fluent 6.2.16.Fluent 6.2.16 Theory's Guide, Fluent Inc. 2004.

Fluent 6.2.16.Fluent 6.2.16 User's Guide, Fluent Inc. 2004.

Hamdad I., Hashemi S., Rossi D., Macchi A.(2007), "Oxygen transfer and hydrodynamics in three-phase inverse fluidized beds", 62, 7399-7405.

Hamidpour M., Chen J., Larachi F. (2012), "CFD study on hydrodynamics in three-phase fluidized beds-Application of turbulence models and experimental validation", Chemical Engineering Science 78, 167-180.

Han H., Lee W., Kim Y., Kwon J., Choi H., Kang Y., Kim S.(2002), "Phase Hold-up and Critical Fluidization Velocity in a Three-Phase Inverse Fluidized Bed", Korean journal of chemical engineering, 20, 163-168.

Jena H.M., (2010), "Hydrodynamics of Gas-Liquid-Solid Fluidized and Semi-Fluidized Beds", Ph.D. Thesis, National Institute of Technology, Rourkela

Jena H.M., Roy G.K. and Meikap B.C., (2008), "Prediction of gas holdup in three-phase fluidized bed from bed pressure drop measurement", Chemical Engineering Research and Design, 86, 1301-1308.

Jena H.M., Roy G.K. and Meikap, B.C. (2005), "Development and Comparative Study of a Semi-Fluidized Bed Bioreactor for Treatment of Wastewater from Process Industries", Process & Plant Engineering -Environment Management, 23, 70-75.

Krishnaiah K., Guru S., Sekar V.(1993), "Hydrodynamic studies on inverse gas–liquid–solid fluidization.", The Chemical Engineering Journal, 51, 109-112.

Lima T.K., "Studies on hydrodynamic behaviour and COD removal efficiency using inverse fluidised bed bioreactor: statistical analysis", Mtech thesis, NIT Rourkela.

Lee K., Son S., Kim U.(2007), "Particle dispersion in viscous three-phase inverse fluidized beds", Chemical engineering science, 62, 7060-7067.

Myre D., Macchi A.(2010), "Heat transfer and bubble dynamics in a three-phase inverse fluidized bed", Chemical Engineering and Processing, 49, 523-529.

Nguyen, K., T., Huang S., C (2011),"Simulation of Hydrodynamic Characteristics of Glass Beads in Gas-Liquid-Solid Three Phase Fluidized Beds by Computational Fluid Dynamics", Journal of Engineering Technology and Education, Vol.-8, No - 2, 248 – 261.

PanneerselvamR., Savithri S., Surender G.D,(2009),"CFD simulation of hydrodynamics of gas–liquid–solid fluidised bed reactor.", Chemical Engineering Science 64, 1119-1135.

Renganathan T. and Krishnaiah, K.(2005), "Voidage characteristics and prediction of bed expansion in liquid–solid inverse fluidized bed", ChemEnggSc, 60, 2545-2555.

Renganathan, T. and Krishnaiah, K.(2004), "Liquid phase mixing in 2-phase liquid–solid inverse fluidized bed", Chemical Engineering Journal 98, 213-218.

Shieh, W. and Keenan, D. (1986), "Fluidized bed biofilm reactor for wastewater treatment, in Advances in BiochemicalEngineering/Biotechnology", Vol 33 ed by Fiechter A. Springer, Berlin Heidelberg, pp, 132-168.

Sokół, W., (2001),"Operating parameter for a gas-liquid-solid fluidized bed bioreactor with a low density biomass support.", Biochemical Engineering Journal 8, 203-212.

Sokół, W., Korpal, W.(2004), "Determination of the optimal operational parameters for a three-phase fluidized bed bioreactor with a light biomass support when used in treatment of phenolic waste waters." Biochemical Engineering Journal 20, 49-56.

Sung, M.S., Suk H. K. , Kim,U., Yong, K., and Sang,D. (2007), "Bubble properties in three-phase inverse fluidized beds with viscous liquid medium", Chemical Engineering and Processing 46, 736-741.

Vijayalakshmi,Balamurugam,Sivakumar,Samuel,Velan.(2000),“Minimum fluidization velocity and friction factor in a liquid-solid inverse fluidized bed reactor.”, Bioprocess Engineering, 22, 461-466.

Zhang J., Epstein N., Grace J. (1998), “Minimum fluidization velocities for gas-liquid-solid three-phase systems”, Powder technology, 100,113-118.

Zhang, J., (1996),“Bubble Columns and Three-Phase Fluidized Beds: Flow Regimes and Bubble Characteristics”, PhD thesis, UBC, Vancouver.

Zhang, X., Ahmadi, G. (2005),“Eulerian-Lagrangian simulation of liquid-gas-solid flow in three- phase slurry reactor.” Chemical Engineering Science ,60, 5089-5104.